ARTICLE IN PRESS

Available online at www.sciencedirect.com

ScienceDirect

Geochimica et Cosmochimica Acta xxx (2021) xxx–xxx

Geochimica et Cosmochimica Acta

www.elsevier.com/locate/gca

A reactive transport approach to modeling cave seepage water chemistry II: Elemental signatures

Jessica L. Oster[a,*], Aaron K. Covey[a], Corey R. Lawrence[b], Max G. Giannetta[c], Jennifer L. Druhan[c]

[a] Department of Earth and Environmental Sciences, Vanderbilt University, Nashville, TN, United States
[b] United States Geological Survey, Denver, CO, United States
[c] Department of Geology, University of Illinois, Urbana-Champaign, IL, United States

Received 8 December 2020; accepted in revised form 30 June 2021; available online xxxx

Abstract

Karst systems are useful for examining spatial and temporal variability in Critical Zone processes because they provide a window into the subsurface where waters have interacted with vegetation, soils, regolith, and bedrock across a range of length and timescales. These hydrologic pathways frequently include the precipitation of speleothems, which provide long-term archives of climate and environmental change. Trace element ratios in speleothems (Mg/Ca, Sr/Ca, Ba/Ca) have the potential to provide information about past changes in rainfall and infiltration, but controls on them can be complex and their interpretation must be based on an understanding of the modern cave system. Here we integrate observations of surface conditions, bedrock, soil, and drip water chemistry of Blue Spring Cave in Tennessee, USA with the reactive transport model CrunchTope, which we have calibrated for karst systems to investigate the primary controls on trace element variations in cave seepage waters. We find that measured drip water Mg/Ca and Sr/Ca are captured within the model through variable amounts of limestone dissolution followed by precipitation of secondary calcite that happens within the cave rather than the host limestone. However, strong spatial controls on drip water Mg/Ca and Sr/Ca likely reflect seepage water interactions with variable amounts of diagenetic phases in the host rock. In contrast, Ba/Ca values are consistent across the cave and vary with effective rainfall, suggesting that this parameter may be the most consistent metric for limestone dissolution and prior calcite precipitation and can act as a proxy for rainfall and infiltration in this cave system. Our findings emphasize the importance of evaluating spatial heterogeneity in cave drip waters and outline a novel modeling approach for determining the dominant controls on drip water chemistry in support of the interpretations of paleoclimate records.

Keywords: Reactive transport; Cave monitoring; Trace elements; Speleothem; Critical zone

1. INTRODUCTION

Although paleoclimate reconstructions from speleothem archives often focus on records of temperature, rainfall, and atmospheric circulation based on $\delta^{18}O$, many studies have utilized trace element proxies to generate valuable information about past hydrologic variability that complements $\delta^{18}O$ records (e.g. Liu et al., 2013; Steponaitis et al., 2015; Oster et al., 2017; Warken et al., 2019). Typically, stalagmite Mg/Ca, Sr/Ca, and less frequently Ba/Ca are interpreted to reflect variations in the degree of prior carbonate precipitation (PCP). PCP refers to carbonate (often calcite, but occasionally aragonite) precipitation occurring on the cave ceiling or in pores, fractures, or conduits within the host rock above the cave (Fairchild and Treble, 2009). Often, if covariation between speleothem

---

* Corresponding author.
E-mail address: jessica.l.oster@vanderbilt.edu (J.L. Oster).

https://doi.org/10.1016/j.gca.2021.06.040
0016-7037/© 2021 Elsevier Ltd. All rights reserved.

Please cite this article in press as: Oster J. L., et al. A reactive transport approach to modeling cave seepage water chemistry II: Elemental signatures. *Geochim. Cosmochim. Acta* (2021), https://doi.org/10.1016/j.gca.2021.06.040

Mg/Ca and Sr/Ca (and less often discussed, Ba/Ca) is observed, these ratios are interpreted to reflect the degree of PCP. The distribution coefficients for Mg and Sr in calcite are much less than 1 so as calcite is precipitated, reduction in drip water Ca concentration is larger than in Mg or Sr concentrations. Thus, as more PCP occurs, drip water Mg/Ca and Sr/Ca increase (Fairchild et al., 2000; Fairchild and Treble, 2009). As PCP should be enhanced when drip waters have more opportunity to degas, higher Mg/Ca and Sr/Ca may be indicative of slower fluid transit times and a drier climate (Fairchild et al., 2000; Johnson et al., 2006). However, ventilation of cave air CO_2 also influences the amount of degassing and PCP of drip waters, leading to changes in Mg/Ca and Sr/Ca that are unrelated to fluid travel times (Banner et al., 2007; Wong et al., 2011). These ventilation changes can also overprint, amplify, or suppress changes in PCP that might arise through variations in water supply (e.g. Oster et al., 2012; Ronay et al., 2019). However, a number of other processes can influence these ratios in stalagmites, including changes in temperature and growth rate, which act on the partitioning of these elements into calcite (Huang and Fairchild, 2001) and contributions of Mg, Sr, and Ba from aeolian and soil sources or other mineral components, such as dolomite, within the host rock (Goede et al., 1998; Wong et al., 2011; Tremaine and Froelich, 2013; Rutlidge et al., 2014; Cross et al., 2015; Oster et al., 2009, 2017).

Numerical models based on observations of elemental variations in cave drip waters and speleothems have been used to disentangle the potential controls on drip water and speleothem Mg/Ca and Sr/Ca (e.g. Fairchild et al., 2000; Wong et al., 2011). Sinclair et al. (2012) proposed a mathematical solution where the slope of a best-fit line through speleothem trace element data plotted as ln(Sr/Ca) versus ln(Mg/Ca) indicates the occurrence of PCP if that slope approaches the value of the ratio of the partition coefficients of Sr and Mg in calcite (D_{Sr}-1/D_{Mg}-1). The I-STAL model incorporates variations in drip rate (as time interval between drips), drip oversaturation, cave pCO_2, and temperature to simulate variations in the degree of water-rock interaction and PCP and how these are recorded in a forward-modeled speleothem (Stoll et al., 2012). Most recently, the model CaveCalc forward-models the soil-karst-cave system as a set of input blocks through the aqueous solution chemistry model PHREEQC (Parkhurst and Appelo, 1999) that can be used to investigate the influences on speleothem trace element variability through a series of linked reactions (Owen et al., 2018). These models provide important insight as to how seasonal variations in temperature, drip rate, and cave ventilation might influence speleothem Mg/Ca and Sr/Ca as well as how surface environmental signals become modified in the subsurface. However, these contributions do not explicitly incorporate the combined effects of advective fluid flow and chemical reactions, thus limiting their utility as forward predictors of the influence of environmental changes on water chemistry in complex karst systems.

We build upon these past contributions and address the limitations mentioned above through the development of a model that couples reactivity and transport to query the soil-karst-cave system. In the first part of this contribution (Druhan et al., 2021), we adapted a reactive transport model (RTM) framework to karst systems by (1) modifying the RTM code CrunchTope (Steefel et al., 2015) to accommodate the three-isotope carbon system (Druhan et al., 2020), and (2) parameterizing this model to simulate the evolution of solute chemistry and carbon isotope ratios in fluids draining through the host rock of the Blue Spring Cave system of Tennessee. We utilize a set of Blue Spring limestone dissolution experiments to constrain kinetic rate and equilibrium constants appropriate to describe water–rock interactions in this system and use this information to drive a 1-dimensional (1D) RTM combining the influences of fluid flow, gas diffusion, and reactivity on carbon isotope transformations within and across the Blue Spring system. The results of this model are detailed in the companion study (Druhan et al., 2021). Briefly, that study utilizes a range of fluid infiltration rates and soil pCO_2 conditions to produce a total of nine simulations comprising the physical conditions appropriate to describe the seasonal variability of the Blue Spring system. Based on this solution envelope, the balance between fluid reactive potential, flow rate and limestone dissolution create a narrow set of parameter combinations in which both the calcium ion concentrations and the radiocarbon content of the fluid emerging from the limestone on the ceiling of the cave fall within the range of measured values. Specifically, the increase in calcium concentrations is matched by a decrease in radiocarbon content as a result of the dissolution of old limestone, such that it is difficult to create a condition in which the drip water calcium concentrations are sufficiently elevated without creating erroneously low radiocarbon contents. A key feature of these results is that the occurrence of PCP within the host rock would promote further dissolution of radiocarbon ‘dead’ limestone. Thus, the model suggests, for the particular conditions at Blue Spring, the occurrence of degassing of CO_2 and PCP within the host rock before water emerges into the cave is inconsistent with measured drip water chemical and isotopic compositions. Here, we extend the CrunchTope RTM framework to investigate the controls on elemental concentration ratios in cave drip waters. Specifically, we consider how Mg/Ca, Sr/Ca, and Ba/Ca change with fluid transport through the system, the potential influence of PCP on these parameters, and how environmental signals should be recorded in speleothems through these ratios.

2. SITE CHARACTERIZATION

Background information about the Blue Spring Cave system (35.96 °N, 85.39 °W, 300 m a.s.l.) is also given in Druhan et al., 2021. Briefly, Blue Spring consists of ~62 km of mapped cave passage within the Mississippian Monteagle Limestone. The Monteagle Limestone is 67–76 m thick in this area and composed of oolitic and skeletal grainstones and packstones, with the dominant skeletal grains being echinoderm and bryozoan fragments (Lumsden et al., 1983). Early diagenesis led to the formation of dolomite, celestite, and fluorite in some paleoenvironments (Handford, 1976). Portions of the cave are overlain by Pennsylvanian sandstones and conglomerates that block infiltrating water and keep much of the cave dry (Matthews and Walter, 2010). However, areas near the edges of cave development and not underneath this cap rock are wet and have substantial active speleothem formation. The climate above Blue Spring is humid subtropical with hot summers and mild winters. Vegetation above Blue Spring consists of deciduous hardwood forest, and soils consist of clay loam on top of clay that has been weathered from limestone and sandstone colluvium. Soil thickness above the cave is highly variable and ranges from 0 to 135 cm or more. Blocks of limestone crop out at the surface or are situated at variable depths below the surface. Rain falls throughout the year in Tennessee, however the late summer through early fall months tend to be the driest (~20% annual precipitation from August to October).

Rainfall in the vicinity of the cave is measured using a HOBO weather station that includes a tipping bucket rain gauge placed at the Cherry Creek Nursery approximately 15 km northwest of Blue Spring Cave. This weather station was operational between December 2013 and March 2017. In August of 2014, another weather station was established just 1 km from the cave. Net rainfall is calculated for both sites, taken to be the difference between precipitation measured at the weather station and potential evapotranspiration, calculated using the Thornthwaite equations after Willmot et al., (1985) and Tremaine and Froelich, (2013). Net rainfall is generally higher and positive during the winter months and negative for much of the summer and fall.

Cave air temperature, relative humidity, and $p\text{CO}_2$ were measured using a handheld device (CO2meter.com) at four locations throughout the cave at each visit from November 2013 to November 2017. These data, as well as information about the carbon isotope signatures of the cave air, are presented in the companion paper (Druhan et al., 2021). Cave air $p\text{CO}_2$ is lowest near the cave entrance and reaches near-surface values in the winter. It increases with distance from the cave entrance within each season. Cave air $p\text{CO}_2$ rises through spring to peak in summer. In the Cathedral Room at the end of the sampling route, which is also the end of this branch of the cave system, $p\text{CO}_2$ reaches up to 1600 ppm during the summer months and falls to ~800 ppm in the winter months. In the Upper Pool Room, where many of our monitoring sites are located, the range of annual variability is slightly lower (640–1350 ppm).

3. METHODS

3.1. Drip and soil water collection and analysis

Drip water was sampled at multiple locations within the cave and analyzed for δ^{18}O, δ^2H, $\delta^{13}\text{C}_{\text{DIC}}$, pH, and cation concentrations. Drip sites that display differing flow characteristics were specifically targeted, including those displaying intermittent and continuous flow, in order to target unique fluid drainage paths through the soil and host rock. Water drips seasonally near the cave entrance, and sites BSw1 and BSw2 were sampled intermittently in this part of the cave beginning in June 2013 (Fig. 1). Site BSw2 became inactive after February 2015 when an ice storm appears to have led to changes in water flow routes that caused this drip location to become dry. The majority of water sample sites are located near the end of the sampling route in the Upper Pool Room, front Cathedral Room, and back Cathedral Room (Fig. 1). Site BSw5 in the Upper Pool Room was sampled from June 2013 through May 2017. Also in the Upper Pool Room, site BSw11 was sampled from August 2014- November 2017. Sites BSw4 and BSw10, located in the front Cathedral Room were sampled from June 2013 to November 2017, and site BSw12, a very slowly dripping site in the back of the Cathedral Room, was monitored from May 2015 to March 2017. Lastly, sites JENC1 – JENC4 in the Upper Pool Room were sampled several times during winter and spring 2017, as part of a targeted effort to investigate spatial heterogeneity in drip rate and water chemistry within a single room of the cave.

Drip water was collected instantaneously at each drip site into precleaned LDPE bottles and then subdivided for each analysis type. At slower drip sites, LDPE bottles were left under the drip at the beginning of the sampling trip and collected on the return trip out of the cave. No bottle was left for more than 1 hour, and no calcite precipitate was ever observed within a collection bottle. Sampling protocols and results for δ^{18}O, δ^2H and $\delta^{13}\text{C}_{\text{DIC}}$ are described in detail in the companion paper (Druhan et al., 2021). Water samples for cation analysis were filtered through 0.2 μm sterile filters and then acidified with concentrated trace metal grade nitric acid to ~2% final HNO_3 concentration. After collection, water samples were transported back to Vanderbilt in a cooler and kept refrigerated until analysis.

Soil water lysimeters are installed above Blue Spring Cave at depths of 30, 50, and 90 cm (L03, L04, L05, respectively). The main site of soil water and gas monitoring has been coordinated via GPS to be above the Cathedral Room at the end of the water sampling route within the cave. This location was chosen so that lysimeters are most likely to capture water infiltrating through the limestone to the monitored portion of the cave. Water was extracted from the lysimeters on a monthly to seasonal basis using a handheld vacuum pump. Further details on the methods and results of soil water analysis are presented in the companion paper (Druhan et al., 2021).

The pH of all water samples was measured at the sampling location using a Fisher-Scientific Accumet pH meter prior to acidification. Cation concentrations in soil water and drip water were measured in solution mode on a Thermo Finnigan iCapQ at Vanderbilt University. Concentration standards were prepared using a custom mixed solution from Inorganic Ventures (Christiansburg, VA) containing Na, Ca, and Mg for high concentration elements and the IV-71A standard solution for low concentration elements. These were mixed online with an internal standard solution (IV-71D). The standard solution IV-Stock-10 was run as an unknown during each analysis period. Each batch of water samples was analyzed over two days, first for lower concentration elements (e.g. Sr, Ba, U), then for higher concentration elements (Ca, Mg). Methods for analyzing O, H, and C isotope ratios in these waters are described in Druhan et al., 2021.

Please cite this article in press as: Oster J. L., et al. A reactive transport approach to modeling cave seepage water chemistry II: Elemental signatures. *Geochim. Cosmochim. Acta* (2021), https://doi.org/10.1016/j.gca.2021.06.040

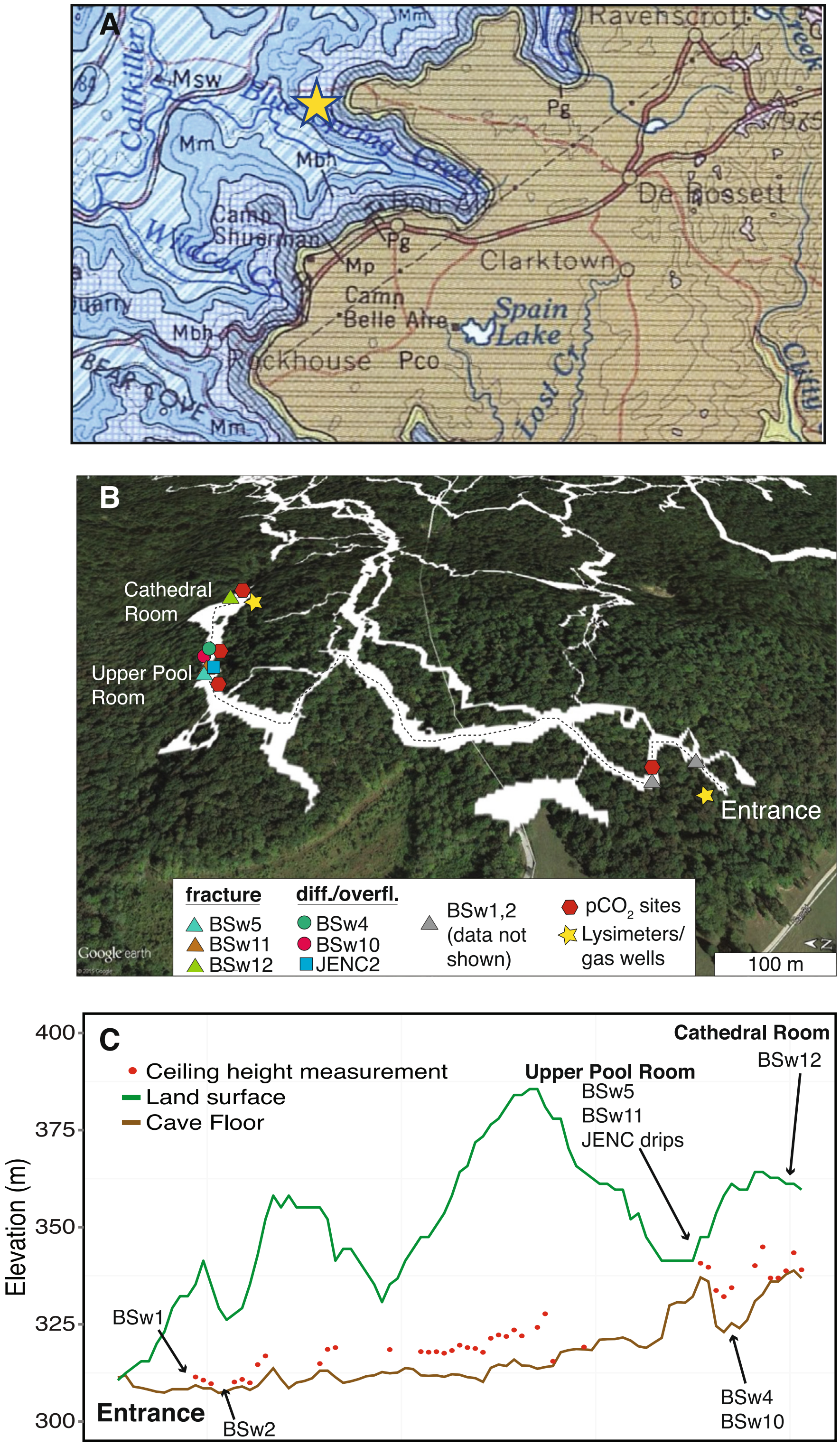

Fig. 1. (A) Geologic map at 1:250,000 scale (Swingle et al., 1966) of area surrounding Blue Spring Cave (yellow star). Map units: Bangor Limestone and Hartselle Formation (Mbh); Monteagle Limestone (Mm); St. Louis Limestone and Warsaw Limestone (Msw); Pennington Formation (Mp); Crab Orchard Mountains Group (Pco). (B) Partial map of Blue Spring Cave overlain on Google Earth image. Dashed line shows route taken for water sampling within the cave. Sites for water sampling and pCO2 monitoring within the cave are marked as are surface lysimeter installations. Cave map is adapted from J. Richards (https://www.rchrds.org/tennesseecarto/2018/1/9/blue-spring-cave). (C) Profile of cave along sampling route shown in B. Measurements of land surface and cave ceiling height from cave cartography work of J. Richards are shown as are sampling sites. Data from water sampling sites BSw1 and BSw2 are not further discussed in the text as these sites became dry partway through the study.

Please cite this article in press as: Oster J. L., et al. A reactive transport approach to modeling cave seepage water chemistry II: Elemental signatures. *Geochim. Cosmochim. Acta* (2021), https://doi.org/10.1016/j.gca.2021.06.040

3.2. Characterization of the host rock, soils, and secondary calcite

Samples of the limestone were collected from ceiling collapse deposits in the Cathedral Room and from blocks exposed on the surface near the location of lysimeter installation. Soil and saprolite samples were also collected from four depths during the installation of lysimeter L03. These samples were sent to Actlabs (Ancaster, ON, Canada) for quantitative X-ray diffraction (XRD) analysis where they were pulverized prior to analysis. A portion of each pulverized sample was mixed with 10 wt% corundum and loaded into a standard holder. Corundum is used as an internal standard in order to determine the amount of amorphous material. The quantities of the crystalline mineral phases were determined using the Rietveld method, which is based on the calculation of the full diffraction pattern from crystal structure information. The X-ray diffraction analysis was performed on a Panalytical X'Pert Pro diffractometer, equipped with a Cu X-ray source and an X'Celerator detector, operating at the following conditions: 40 kV and 40 mA, range 5–80° 2θ; step size 0.017° 2θ, time per step 50.165 sec, fixed divergence slit, angle 0.5°, and sample rotation 1 rev/sec.

Further characterization of the host limestone was conducted via petrographic analysis of thin sections. Lastly, the trace element composition of the host limestone was analyzed using a Photon Machines Excimer laser coupled to a Thermo Finnigan iCapQ quadrupole ICP-MS at Vanderbilt University. Portions of skeletal fragments and cements across three thin sections through fresh unweathered limestone were targeted for elemental analysis. Laser ablation analysis was also carried out in order to characterize the trace element content of secondary calcite precipitating within the cave. For this, we used a broken stalagmite that was found lying next to its base within the Cathedral Room close to the location of drip site BSw12. This stalagmite has been dated to ~120,000–80,000 cal yrs BP using U-Th dating methods (unpublished data). Trace element concentrations were analyzed along the growth axis of the stalagmite. Analyses were conducted as line scans using a 20 X 100 μm rectangular slit at a scan speed of approximately 5 μm/s at 20% laser power and a repetition rate of 10 Hz. The line scans followed a pre-ablation step that was conducted over the sample path at a scan speed of 10 μm/s at 50% laser power at a repetition rate of 15 Hz. The multi-element synthetic glass standard NIST SRM 612 was used for elemental quantification using ^{44}Ca. The synthetic pressed aragonite powder standard MACS3 was also analyzed at the beginning and end of each run. The laser ablation data were processed using the Iolite software package (Paton et al., 2011). For the purposes of this study, only the mean and range of stalagmite Sr/Ca and Mg/Ca was used to place constraints on the trace element content of the secondary calcite phase that is precipitating within the host rock and the cave.

3.3. Batch dissolution experiments

A series of limestone dissolution experiments were conducted to constrain the rates and equilibria appropriate to this particular carbonate for parameterization of the reactive transport model. The details of this experimental methodology are provided in the companion paper (Druhan et al., 2021). Briefly, a known mass of limestone with constrained surface area collected from Blue Spring Cave was submerged in atmospherically equilibrated deionized (DI) water (pCO_2 400 ppmv, pH 5.8) and sealed in a closed vessel subject to constant stirring and a fixed temperature of 22 °C. Fluid samples were collected at known time intervals, and the resulting evolution of the solute chemistry was used to constrain a reaction network model including appropriate equilibria for the carbonate system and pH during a kinetically controlled dissolution of the limestone to reach an effectively equilibrated system. Cation concentrations including Ca, Mg and Sr were measured by inductively coupled mass spectrometry at the University of Illinois Urbana-Champaign

4. RESULTS

4.1. Host rock and secondary carbonate composition

The mineralogy of the host limestone samples was verified via quantitative XRD to consist primarily of calcite (88.6 wt% calcite, 3.4 wt% quartz, 1.2 wt% mica, 6.8 wt% amorphous solids). Saprolite and soils consist primarily of quartz (70–88 wt%) with some amorphous phases (11–28 wt%) and small amounts of mica (trace to 2 wt%). Petrographic analysis of the limestone confirms, consistent with previous analyses of the Monteagle Limestone (Lumsden et al., 1983; Driese et al., 1994), that the Blue Spring host rock is characterized by numerous echinoderm and bryozoan fragments and ooids surrounded by carbonate cements. Laser ablation ICP-MS indicates on average lower Mg/Ca, Sr/Ca, and Ba/Ca for cements than the skeletal fragments. Averaged laser ablation ICP-MS results for the limestone and the stalagmite collected from the Cathedral Room are given in Table 1.

4.2. Drip water cation concentrations

Monitored drip sites within Blue Spring Cave display three main types of beha chemical variability, as fracture-fed drips show a wider rangvior in terms of drip rate and geochemical variability. We refer to drip sites that display a large range of drip rates, respond rapidly to rainfall events, and become seasonally dry as *fracture-fed drips* (BSw5, BSw11, BSw12, JENC3, JENC4). As a point of reference, fracture fed drips have exhibited volumetric flow rates as high as 200 ml/min. Drips that do not seasonally dry up and display more gradual variations in drip rate are referred to as *diffuse flow drips* (JENC1, BSw4, BSw10). As a comparison, these diffuse drips have been observed to produce flow rates of 5–10 ml/min. These values are consistent with the 'group 1′ seasonal drip rates reported by Miorandi et al., (2010) for a cave system located in a Mediterranean climate. Lastly, drip site JENC2 displays what we characterize as overflow behavior, showing smaller and more gradual responses to some rainfall events, but much larger changes in drip rate in response

Please cite this article in press as: Oster J. L., et al. A reactive transport approach to modeling cave seepage water chemistry II: Elemental signatures. *Geochim. Cosmochim. Acta* (2021), https://doi.org/10.1016/j.gca.2021.06.040

Table 1
Laser ablation ICP-MS results for host rock and stalagmite.

Component	Avg Mg/Ca (mmol/mol)	SD	Avg Sr/Ca (mmol/mol)	SD	Avg Ba/Ca (mmol/mol)	SD
All Host Limestone ($n = 38$)	14.8	3.2	0.81	0.3	1.00E−03	0.0007
Cements ($n = 8$)	13.6	3.0	0.61	0.3	6.00E−04	9.08E−04
Skeletal fragments ($n = 38$)	15.1	3.2	0.85	0.27	1.30E−03	6.91E−04
Stalagmite	2.19	0.81	0.133	0.03	3.80E−03	1.10E−03

to large or sustained rainfall events (Fairchild and Treble, 2009; Baker et al., 2012). Drip character can also be distinguished on the basis of chemical variability, as fracture-fed drips show a wider range of variability in $\delta^{18}O$, $\delta^{2}H$, and $\delta^{13}C_{DIC}$ values; this distinguishing behavior is further described in the companion paper (Druhan et al., 2021).

Drip water Mg/Ca, Sr/Ca, and Ba/Ca (all ratios reported in mmolX/molCa) show complex behavior across drip sites and through time (All drip water data reported in Table S1). Mg/Ca and Sr/Ca values generally covary across all drip sites ($r_s = 0.74$, $p < 0.001$, $n = 133$), whereas Sr/Ca and Ba/Ca show a moderate positive correlation ($r_s = 0.40$, $p < 0.001$, $n = 133$), and Mg/Ca and Ba/Ca have a weak positive correlation ($r_s = 0.20$, $p < 0.05$, $n = 133$). Positive correlations between Mg/Ca, Sr/Ca, and Ba/Ca are often interpreted to reflect the influence of variable amounts of PCP along the seepage water flow path up to the point of drip water collection or speleothem precipitation (Fairchild and Treble, 2009). Sinclair et al., (2012) proposed, if PCP were the primary control on drip water and speleothem element to calcium rations, that cross plots of ln(Sr/Ca) versus ln(Mg/Ca) and ln(Ba/Ca) should follow a theoretical slope defined by the partition coefficients of each element between calcite and water equal to $(D_i - 1)/(D_j\text{-}1)$ where i and j = Mg, Sr, and Ba. For published values of D_{Mg}, D_{Sr}, and D_{Ba} (Huang and Fairchild, 2001; Tesoriero and Pankow, 1996), this results in slopes of ~0.88 for the relationship between ln(Sr/Ca) and ln(Mg/Ca) (Sinclair et al., 2012) and ~1.16 for the relationship between ln(Sr/Ca) and ln(Ba/Ca) (Warken et al., 2019).

A graphical comparison between ln(Sr/Ca), ln(Mg/Ca), and ln(Ba/Ca) for the Blue Spring drip water indicates that the waters plot along lines of similar slopes to those theoretical values (Fig. 2). This is especially apparent for the comparison of ln(Sr/Ca) and ln(Ba/Ca). However, it is also apparent that the drip waters fall along more than one line of similar slope to the theoretical PCP-controlled value. All drip analyses have similar or overlapping values of Ba/Ca, and the different trends between drip sites reflect variations in the overall value of Sr/Ca. In a graphical comparison of drip water ln(Mg/Ca) versus ln(Sr/Ca), water samples are more closely aligned with the theoretical PCP slopes (varying between 0.88 and 0.9 (Sinclair et al., 2012)) than with the theoretical line of calcite recrystallization (Fig. 2). However, drip water values also suggest slopes that are steeper than the theoretical PCP slopes, indicating a greater variation in Sr/Ca than can be attributed to changes in PCP alone.

We can also examine changes in ln(Mg/Ca), ln(Sr/Ca), and ln(Ba/Ca) through time. For much of the record, diffuse flow sites display higher and less variable Mg/Ca than fracture or overflow sites (Fig. 3). However, from early 2014 to mid-2015, this behavior changes and both fracture and diffuse flow sites display large variations in Mg/Ca. This interval of highly variable drip Mg/Ca occurs at a time when net rainfall is also highly variable (Fig. 3). Similar behavior is evident in the record of Sr/Ca through time. However, from September 2015 to the end of the record, it is apparent that different drips fluctuate around different mean values of Sr/Ca, with site BSw12 having the highest Sr/Ca, followed by BSw4 and BSw10, then BSw5 and BSw11. These values largely follow the spatial locations of the drips within the cave (Fig. 1). If we separately examine ln(Sr/Ca) drip waters collected before and after September 2015, this geographic separation is apparent (Fig. 4). Tremaine and Froelich (2013) suggested that drip waters should plot along linear vectors in Mg/Ca versus Sr/Ca space, with slopes determined by starting host rock composition if PCP was a dominant influence on drip water chemistry. In Fig. 5, we explore the influence of drip type and temporal changes in water flow on element to calcium ratios by separating the drip sites into diffuse (panels A and B) and fracture and overflow (panels C and D) sites, and by shape coding the points by pre- and post-September 2015. Following Tremaine and Froelich (2013) and Wassenburg et al., (2020), we add two modeled PCP vectors to panels B and D that would represent generic host rock compositions of 80 %limestone/20 %dolomite and 60 %limestone/40 %dolomite. Through this analysis, it is apparent that this temporal separation does not explain much of the variation that we observe in drip water chemistry. It is also clear, while the addition of more dolomite to the host rock mixture may explain some of the higher Mg/Ca values that we observe, that changes in the amount of dolomite cannot explain the wide range of Sr/Ca values that we measure, necessitating perhaps the addition of other host rock phases that would elevate Sr/Ca at certain drip sites. This same wide range of Sr/Ca is also apparent in panels A and C.

4.3. Trace element batch experiments

We consider the time series release of trace elements magnesium (Mg^{2+}) and strontium (Sr^{2+}) to solution over the course of the limestone dissolution experiment as a further constraint on the dynamics of water–rock interaction in the Blue Spring system. Importantly, the dissolution of these two nominally trace elements is driven by the solubility of the limestone sample, which is a function of the saturation state of the fluid (i.e. the pH, calcium, and

Please cite this article in press as: Oster J. L., et al. A reactive transport approach to modeling cave seepage water chemistry II: Elemental signatures. *Geochim. Cosmochim. Acta* (2021), https://doi.org/10.1016/j.gca.2021.06.040

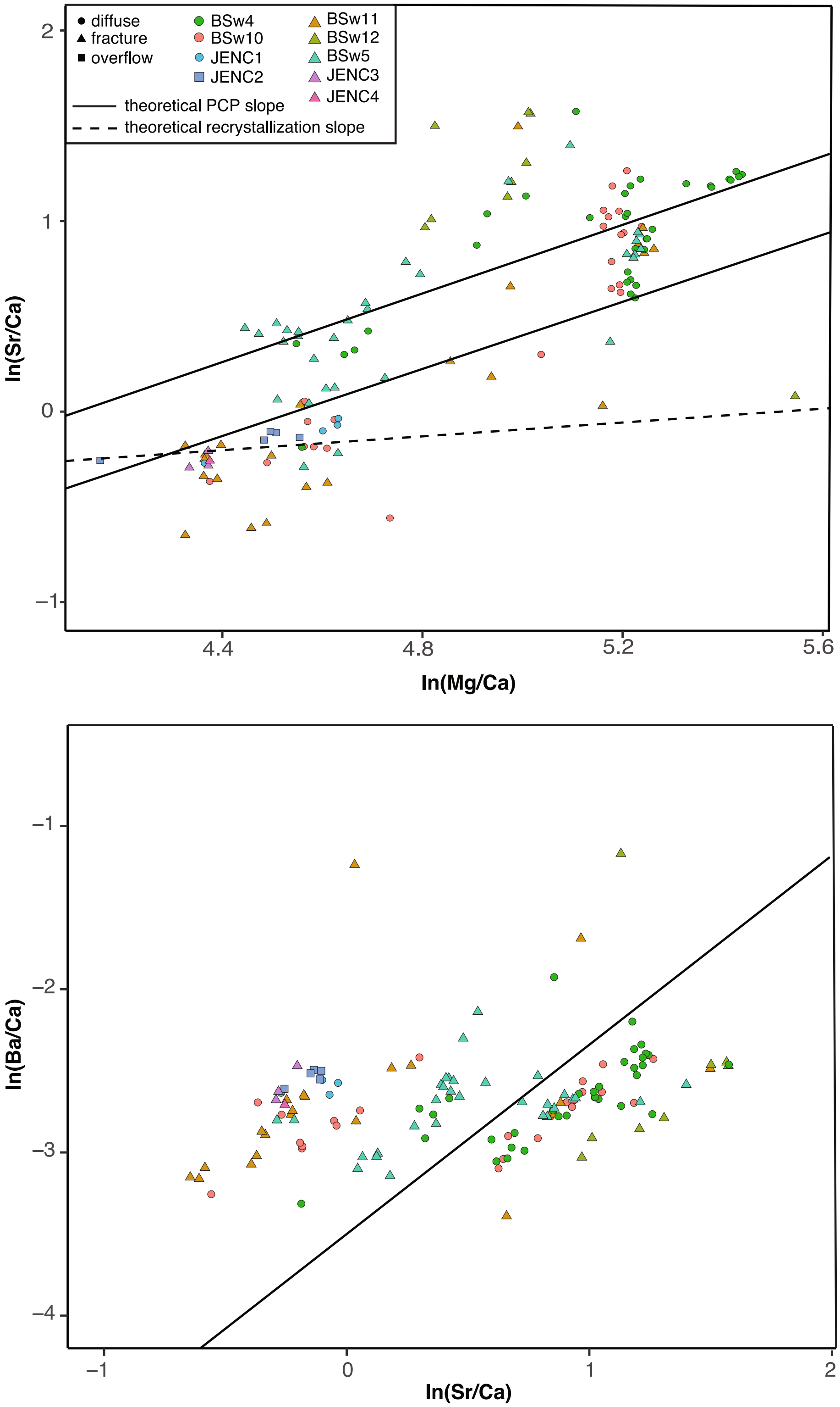

Fig. 2. Top panel, ln(Mg/Ca) versus ln(Sr/Ca) for Blue Spring drip waters coded by drip site (color) and drip type (shape). Solid lines depict range of theoretical PCP slopes, and dashed line represents the theoretical calcite recrystallization slope (after Sinclair et al., 2012). Bottom panel, same as top for ln(Sr/Ca) versus ln(Ba/Ca).

dissolved inorganic carbon concentrations). In this sense the prevalence of Mg and Sr in solution has negligible effect on the dissolution rate, and these two trace elements are effectively carried along by the equilibria of the major element stoichiometry. Thus, the rate and equilibria constrained by these batch experiments is documented in

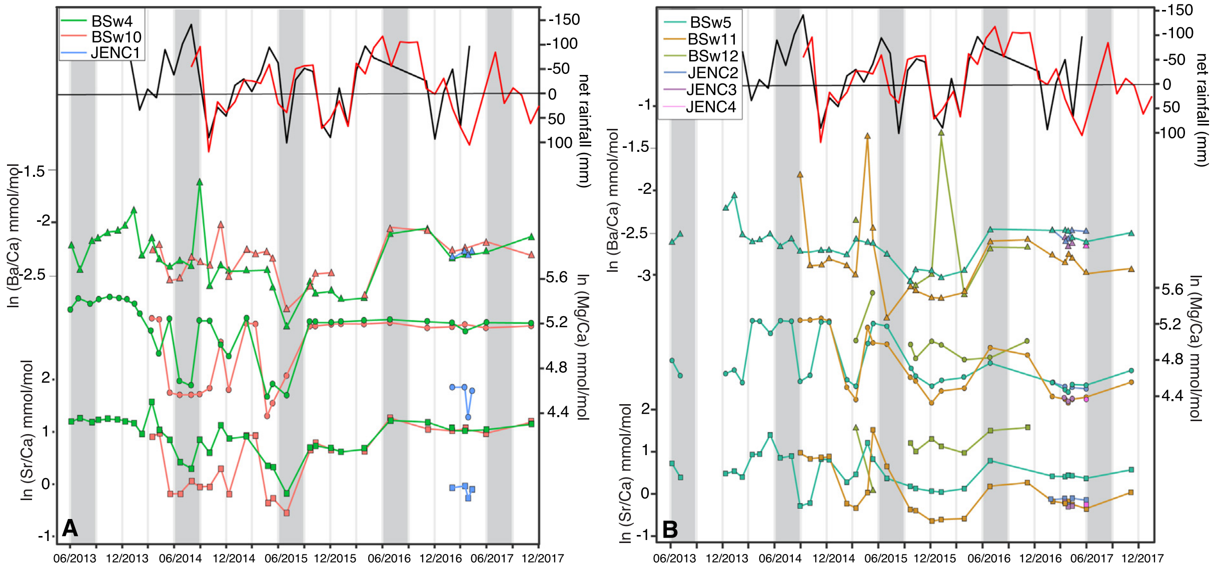

Fig. 3. From top to bottom, time series of net rainfall calculated based on the Cherry Creek weather station (black) and the Blue Spring weather station (red) (note reversed y-axis); time series of drip water Ln(Ba/Ca); Ln(Mg/Ca); Ln(Sr/Ca) color-coded by drip site (color) for June 2013 through December 2017. Panel A shows sites characterized as diffuse flow drips. Panel B shows sites characterized as fracture flow or overflow (JENC2) drips. Grey shading highlights the summer seasons (June, July, August) for each year.

the companion paper (Druhan et al., 2021) in the context of calcium and dissolved inorganic carbon analysis (Eq. (1)):

$$\frac{dC}{dt} = kA\left(1 - \frac{C}{C_{eq}}\right) \tag{1}$$

Here, the rate constant (k), surface area (A), and equilibrium concentration (C_{eq}) for the dissolution experiment are the same as those reported in the companion study. The stoichiometry of the limestone is simply expanded to include the incorporation of these trace elements as small substitutions for calcium based on the ratios obtained from the batch dissolution experiment and confirmed by laser ablation of the limestone:

$$\begin{aligned} &Ca_{0.97513408}Mg_{0.02437835}Sr_{0.00048757}CO_3 \\ &\times \overset{K_{eq}}{\leftrightarrow} 0.97513408Ca^{2+} + 0.02437835Mg^{2+} \\ &+ 0.00048757Sr^{2+} + 1.000CO_3^{2-} \end{aligned} \tag{2}$$

This stoichiometry creates an aqueous Mg/Ca ratio of 25 mmol/mol and a Sr/Ca ratio of 0.5 mmol/mol. Thus, the calcium and dissolved inorganic carbon systems drive the release of Mg and Sr into solution, while the presence of these trace phases is assumed to exert negligible effects on the dynamics of calcium and dissolved inorganic carbon in the system.

The results from the batch reactors show how the evolution of these two elements differs through time. Mg^{2+} concentrations are highly variable, averaging approximately 44 ppb with a general trend towards higher concentrations through time but with many unstable peaks and drops in concentration (Fig. 6A). The corresponding Mg/Ca ratio (reported in mmol/mol) is equally variable, with an extremely high value early in the experiment (466 after the first 5 minutes of the experiment) dropping down to a relatively stable value of approximately 20 as the system equilibrated. In contrast, Sr^{2+}concentrations progress in lock step with Ca^{2+}, increasing to an equilibrium value of 4.7 ppb, and adhere to precisely the same simplified dissolution rate expression (Eq. (1)) as Ca^{2+} for the same rate constant and surface area (Fig. 6B; Druhan et al., 2021). The corresponding Sr/Ca ratio is extremely stable, reaching a value of approximately 0.5 after the first few hours of the experiment and remaining level thereafter. Notably, the same simplified TST model (Eq. (1)) with the parameter values that accurately reproduce Ca^{2+} and Sr^{2+} fails to even reach the same order of magnitude in Mg^{2+} concentrations.

In total these results indicate that the release of Sr^{2+} and Ca^{2+} into solution are subject to the same governing processes, while the solubilization of Mg^{2+} from this limestone must be influenced by additional processes which do not appear to exert significant influence on the other cations. One possibility is the precipitation of some secondary phase which influences the concentration of Mg^{2+}. In the experimental system, we consider this influence negligible as a result of the saturation calculations (Druhan et al., 2021) indicating that the system does not achieve conditions in which calcite would begin to precipitate. In addition, the close association of Sr^{2+} and Ca^{2+}, most notably through their contemporaneous time evolution and stable ion ratio (Fig. 6B) suggests negligible precipitation of any secondary phase that would exert a partitioning between them. Thus, the extremely high Mg/Ca ratio and variable Mg^{2+} concentrations of this system would more reasonably be associated with a combination of incongruent release into solution or the presence of a rapidly dissolving high Mg^{2+} carbonate phase.

Please cite this article in press as: Oster J. L., et al. A reactive transport approach to modeling cave seepage water chemistry II: Elemental signatures. *Geochim. Cosmochim. Acta* (2021), https://doi.org/10.1016/j.gca.2021.06.040

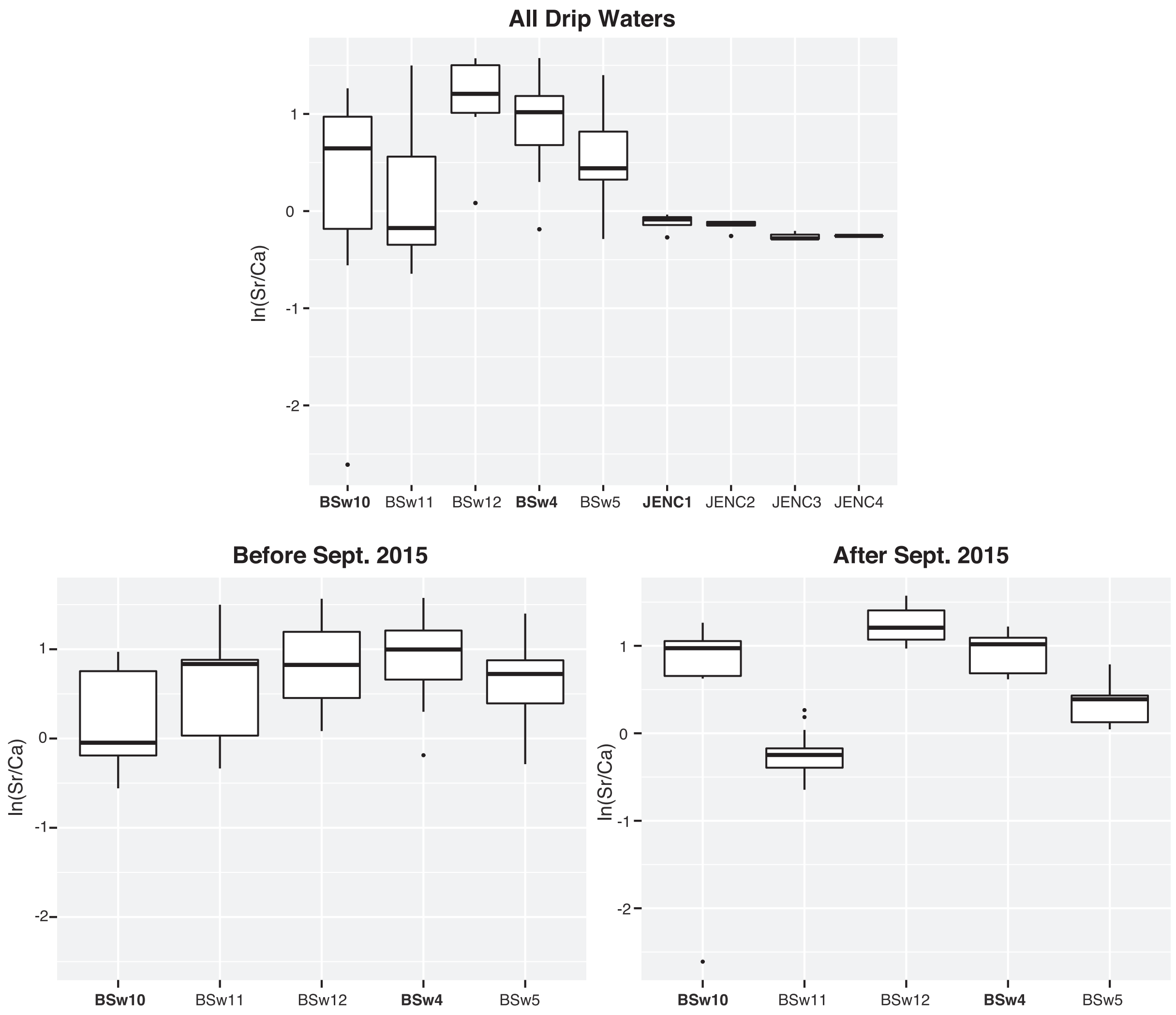

Fig. 4. Boxplots illustrating range of ln(Sr/Ca) values by drip site for all sampled waters (top); waters collected prior to September 1st 2015 (bottom left), and waters collected after September 2015 (bottom right). Waters from JENC sites were only collected after September 2015 and are only shown on the top panel. Labels for diffuse drip sites are shown in bold.

By hand sample and petrographic analysis of thin sections, it is evident that the Blue Spring limestone is rich in crinoids, which build shells out of high-Mg calcite. In order to approximate the possible influence of a high Mg/Ca phase or preferential Mg^{2+} release, we incorporate a minor volume of a second mineral in the CrunchFlow simulations, with the following stoichiometry:

$$Ca_{0.6818}Mg_{0.3178}Sr_{0.0004}CO_3 \overset{K_{eq}}{\leftrightarrow} 0.6818Ca^{2+} + 0.3178Mg^{2+} + 0.0004Sr^{2+} + 1.000CO_3^{2-} \quad (3)$$

We wish to emphasize that we are not suggesting that this specific high Mg/Ca phase actually exists in the system, but rather this hypothetical mineral is included in order to reproduce the effects of incongruent dissolution or the presence of high Mg/Ca phases in the model. Through this approach, we can add an extremely small amount of this mineral to the prior simulations (0.0001 volume fraction) and, assuming an identical surface area as the limestone, implement a distinct equilibrium and rate constant ($10^{-14.8}$ and $10^{-3.6}$ mol/m^2/yr, respectively) in order to drive rapid initial dissolution of this phase. The model output from this simulation reproduces the observed Mg/Ca ratio of the experiment (Fig. 7A) with insignificant impact on the concentration or ion ratio time series of Ca^{2+} and Sr^{2+} (Fig. 7B).

The result of this exercise is a numerical reaction network model calibrated to the early dissolution of the Blue Spring host limestone reacting with dilute acidic water for a sample with a reasonably low mineral surface area, comparable to field conditions. The simulations incorporate the complete carbonate equilibria in the evolving calculation of saturation state and are executed for a partially saturated system such that equilibration with gas phases and the corresponding change in $CO_{2(g)}$ partial pressure are tracked. This allows us to demonstrate, as expected from theoretical considerations, that simple dissolution of this solid phase is not sufficient to saturate with respect to secondary calcite; thus, the reactive transport processes of the cave system must alter the fluid beyond what is captured here. In addi-

Please cite this article in press as: Oster J. L., et al. A reactive transport approach to modeling cave seepage water chemistry II: Elemental signatures. *Geochim. Cosmochim. Acta* (2021), https://doi.org/10.1016/j.gca.2021.06.040

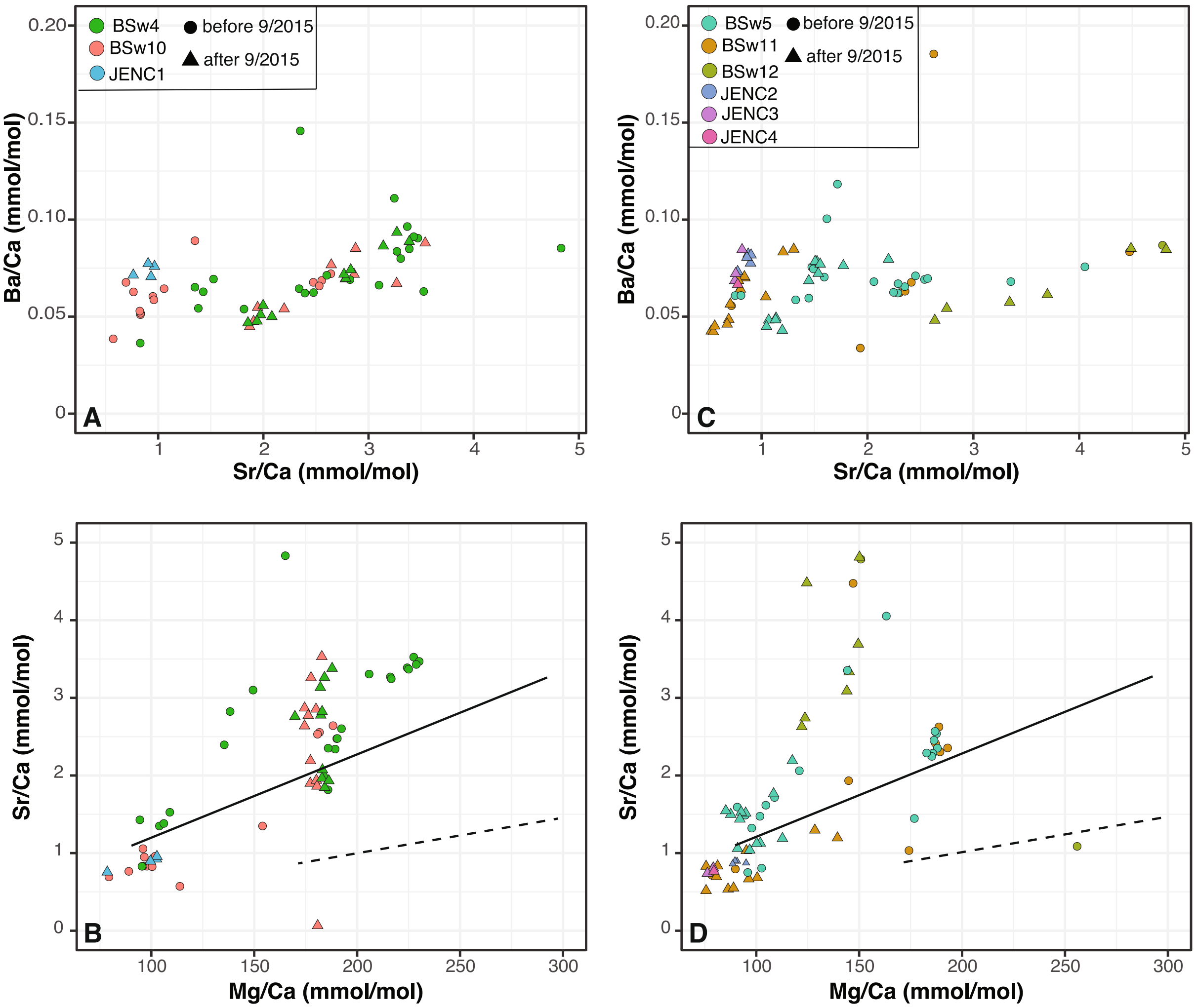

Fig. 5. For diffuse flow drips (A, B) and fracture flow and overflow drips (C, D): A and C show Sr/Ca versus Ba/Ca, B and D show Mg/Ca versus Sr/Ca. Drip waters are color coded by drip site. Samples collected before September 2015 are coded as circles and those collected after September 2015 are coded as triangles. On bottom panels, solid lines represent modeled PCP vectors with a starting host rock composition of 80% limestone/20% dolomite. Dashed lines represent PCP vectors with starting host rock composition of 60% limestone/40% dolomite. PCP vectors are calculated following Wassenburg et al (2020) and Tremaine and Froelich (2013).

tion, we treat a more complex evolution of Mg^{2+} as a potentially important tracer given its unique behavior relative to both Ca^{2+} and Sr^{2+} through time.

5. DISCUSSION

5.1. Observations of Mg/Ca, Sr/Ca, and Ba/Ca in the modern system

Covariation between Mg/Ca and Sr/Ca in stalagmites and drip waters is often used to diagnose PCP in karst systems (Fairchild et al., 2000; Sinclair et al., 2012; Tremaine and Froelich, 2013). However, for this covariation to be apparent, Mg and Sr must be supplied by a single source to the seepage water, or contributions from multiple sources must be understood and taken into account (Tremaine and Froelich, 2013). Although Blue Spring drip waters plot on similar slopes in ln(Mg/Ca) versus ln(Sr/Ca) space as those proposed to reflect PCP (Sinclair et al., 2012), the drip waters plotting on multiple linear trends with similar slopes indicates that both Mg and Sr may be supplied to the drip water by multiple phases within the Monteagle Limestone. The results of the batch dissolution experiment point to a secondary phase that rapidly contributes Mg to solution from the fresh cut surface of the hand sample. Petrographic analysis of thin sections confirms the presence of crinoid fragments within the limestone, which are echinoderms composed of high-Mg calcite. Furthermore, previous examination of the Monteagle Limestone has indicated the presence of diagenetic dolomite (Handford, 1976). Thus, it is possible that differential dissolution of high-Mg calcite, which tends to react more easily than low-Mg calcite (Busenberg and Plummer, 1989) or dolomite, which reacts more slowly than calcite (Chou et al., 1989) may be variably contributing Mg to the Blue Spring seepage waters. However, the different

Please cite this article in press as: Oster J. L., et al. A reactive transport approach to modeling cave seepage water chemistry II: Elemental signatures. *Geochim. Cosmochim. Acta* (2021), https://doi.org/10.1016/j.gca.2021.06.040

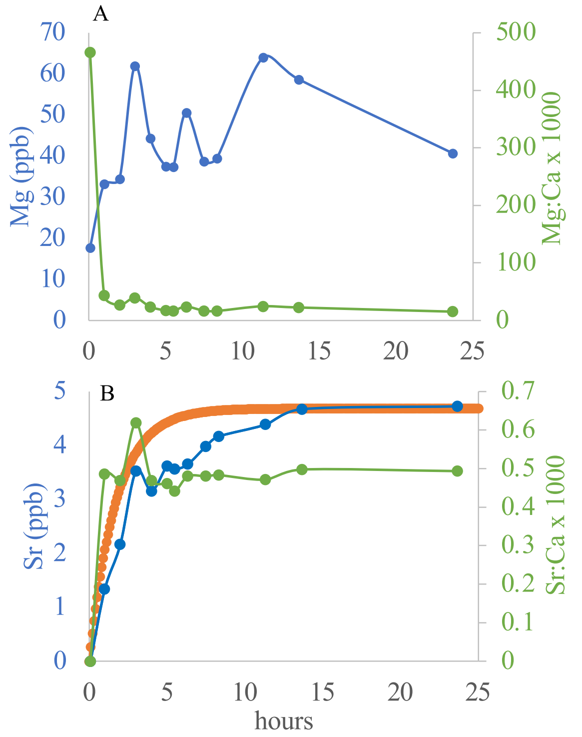

Fig. 6. Fluid chemistry as a function of time during closed system dissolution of a Blue Spring limestone sample. (A) Mg^{2+} (blue) and Mg:Ca molar ratio (green) evolution over 24 hours of continuous reaction; (B) Sr^{2+} (blue) and Sr:Ca molar ratio (green) evolution over the same period. Orange line in (B) illustrates the fit of a simple first-order TST rate expression, described further in the companion paper (Druhan et al., this issue, Electronic Annex). This simple TST rate law describes both the Sr time series (panel B) and the Ca time series (Druhan et al., this issue) for a common set of parameters (rate constant, mineral surface area). However, the same rate law produces Mg concentrations that are at least an order of magnitude too low to match the observed Mg time series. In panel A, the same model would appear as a horizontal line plotting at y = 0 on the left axis relative to the 20–60 ppb Mg concentrations plotted in blue. (For interpretation of the references to colour in this figure legend, the reader is referred to the web version of this article.)

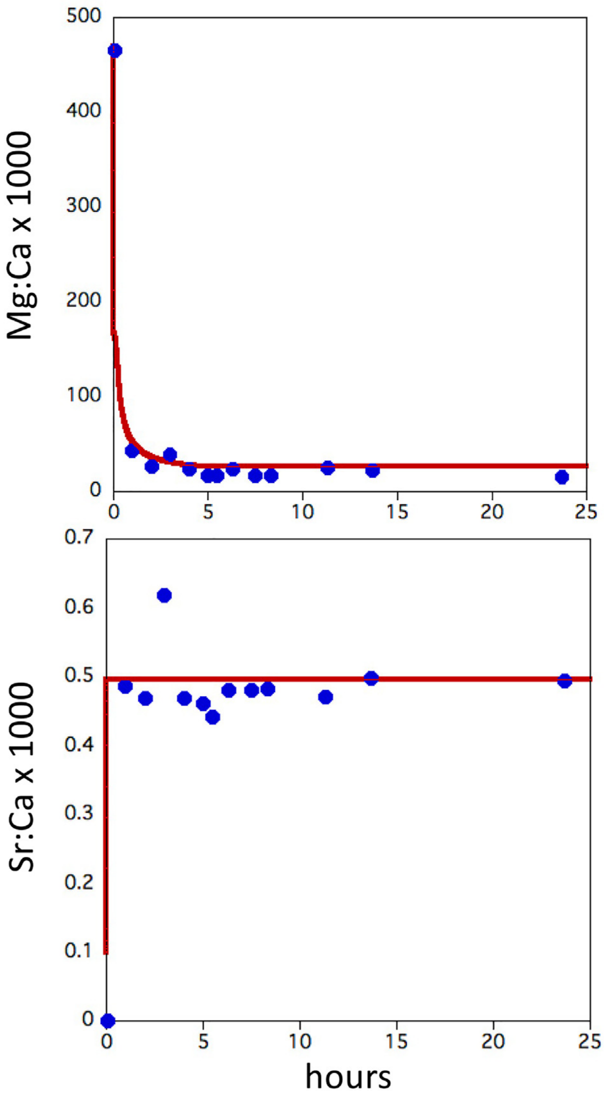

Fig. 7. Fluid chemistry as a function of time during closed system dissolution of a Blue Spring limestone sample. Top panel: Mg:Ca molar ratio (blue points) evolution over 24 hours of continuous reaction with contemporaneous CrunchTope simulation (red); Bottom panel: Sr:Ca molar ratio (blue points) evolution and CrunchTope simulation (red) over the same period. (For interpretation of the references to colour in this figure legend, the reader is referred to the web version of this article.)

behavior of Mg and Sr in the dissolution experiment indicates that any high-Mg phase is not also supplying additional Sr to the seepage water. It is also evident from Fig. 5 that varying the proportion of dissolved limestone versus dolomite cannot explain the range of measured drip water Sr/Ca (Fig. 5).

There is apparent spatial variability in drip water Sr/Ca (Figs. 4 and 5). For much of the monitoring period, and especially from September 2015 to the end of the record, sites BSw11 and the adjacent JENC sites display the lowest Sr/Ca, followed by nearby BSw5, then sites BSw4 and BSw10, which are very close to each other, and lastly BSw12 at the end of the sampling route has the highest Sr/Ca. Similarly, early in the monitoring study between June 2013 and March 2014, site BSw4 showed much higher Sr/Ca than BSw5. However, between March 2014 and September 2015, both Sr/Ca and Mg/Ca show high variability among all drip sites (Fig. 3). This interval corresponds to one of highly variable net rainfall.

Unlike Mg, the release of Sr from the limestone during the batch dissolution experiment very closely followed Ca (Fig. 6). This suggests that if an accessory phase is contributing Sr to the drip water, it was not present in the limestone sample used for the batch dissolution experiment. Celestite associated with diagenesis has been noted in the Monteagle Limestone (Handford, 1976). Thus, we consider the hypothesis that a heterogeneously distributed Sr-rich reactive phase, hereafter referred to as “celestite” is contributing Sr to the drip water. Further, we hypothesize that the seepage water that reaches sites BSw4, BSw10, and

Please cite this article in press as: Oster J. L., et al. A reactive transport approach to modeling cave seepage water chemistry II: Elemental signatures. *Geochim. Cosmochim. Acta* (2021), https://doi.org/10.1016/j.gca.2021.06.040

BSw12 typically accesses flow paths that contain higher amounts of the diagenetic celestite and dolomite phases than the seepage water that supplies sites BSw5, BSw11, and the JENC sites in the Upper Pool Room. However, it is possible that large changes in infiltration, such as those that may have altered flow paths between March 2014 and September 2015, could result in variable access to these diagenetic phases for the water reaching all drip sites.

In contrast to Mg/Ca and Sr/Ca, Ba/Ca displays very similar values and behavior between all drip sites (Fig. 3) suggesting it is likely supplied from a single source within the soil-host rock system and not modified by addition from heterogeneously distributed diagenetic phases. In addition, Ba/Ca at all sites shows variations that align with changes in net rainfall (Fig. 3). These observations are consistent with the occurrence of PCP that varies due to changes in water infiltration and fluid flow, with more PCP occurring during drier intervals (e.g. Fairchild et al., 2000; Warken et al., 2019). Accounting for differences in mean values between drip sites, similar variability is apparent in Sr/Ca and in Mg/Ca for all but BSw4 and BSw10, especially after September 2015 (Fig. 3).

This comparison of the drip water measurements and the batch dissolution experiment indicates that PCP may represent a secondary control on Sr/Ca and Mg/Ca but is a primary control on Ba/Ca in the Blue Spring system. In the following sections, we use the RTM to further evaluate these hypotheses and explore the roles of limestone and accessory phase dissolution and secondary calcite precipitation on the evolution of drip water chemistry and how these relate to fluid flow.

5.2. Reactive transport simulations

5.2.1. Base case model and host rock dissolution

Our 1D reactive transport model development and validation is documented extensively in the companion paper (Druhan et al., 2021) and all parameter values are reported therein, with the exception of the updated mineral stoichiometry described in Section 4.3. The carbon isotope study emphasized the spatiotemporal patterns of calcium, radiocarbon, and $\delta^{13}C$ of dissolved inorganic carbon across the host rock through a combination of nine pairs of fluid flow rates and soil pCO_2 conditions (Fig. 8a, b). Here, we instead focus on the elemental ratios of the simulated fluid exiting the base of the limestone, at the cave boundary, under similar variations in flow rate and pCO_2, as a representation of drip water chemistry in Blue Spring Cave (Fig. 8c, d). Each of the simulated values is obtained from a unique 1D model, run forward in time from initial conditions to a fixed volume of fluid advected through the system. For our slowest flow rates, we run the simulation for 4000 days, and for our fastest rates this simulation is run to 1000 days. In all cases, this is well beyond the time necessary to remove any effects associated with the choice of initial conditions necessary to launch this forward model. Critically, this does not imply that it takes this long for fluid to traverse the distance from the soil, through the limestone, and into the cave. Rather, the slowest flow rate is 25% that of the fastest; thus, comparison of these two time windows allows a comparable volume of fluid to have moved through the system. Over these timescales, the initial condition of the simulation is completely erased from the fluid, and the simulation has reached a stable distribution in solute chemistry.

The model reported in Druhan et al., 2021 is simplified in the current application in that the isotopes of carbon are no longer explicitly tracked. Instead, the trace incorporation of Mg and Sr in the limestone is included (Eq. (2)) as well as a small amount of the high-Mg crinoid phase with rate constant and equilibria determined from the batch reaction experiments (Eq. (3); Fig. 7). The upper boundary condition fluid solutes include both Mg and Sr, such that for the same Ca concentration implemented in the companion study, the Mg/Ca ratio is 144 mmol/mol and the Sr/Ca ratio is 1.36 mmol/mol in agreement with the mean values measured in the deepest lysimeter (L05) above the Cathedral Room. These values are much higher than the elemental ratios of the host limestone, resulting in the expectation that both ratios will decrease in the cave drip water relative to this upper boundary condition as a result of the extent to which the limestone signature is incorporated into the fluid.

When evaluating these parameters into the 1D reactive transport framework, it is apparent that the long-term impact of implementation of the high-Mg crinoid phase was effectively negligible. This is consistent with the batch reactor data (Figs. 6a & 7a) which indicate that this substantially elevated Mg/Ca ratio is rapidly overwhelmed by the lower ratio of the limestone (Fig. 8). In the 1D framework, this translates into a complete loss of the high Mg/Ca ratio imparted by the crinoid before the fluid has even traversed the upper few centimeters of the epikarst, regardless of the choice of flow rate. Thus, this extraordinarily brief, transient feature noted in the batch reactors becomes negligible across the spatiotemporal scale of the Blue Spring system.

The results of the nine simulated parameter pairs (three flow rates, three soil pCO_2 conditions) produce a range of Mg/Ca and Sr/Ca in the drip water entering the cave that are tightly grouped relative to drip water measurements (Figs. 8 and 9), with higher pCO_2 values and slower flow resulting in relatively more limestone dissolution and lower Mg/Ca and Sr/Ca values (Fig. 8). Critically, these ratios show good agreement with the lowest cluster of ratios measured in the drip water. This is an important observation as it suggests that the ratios observed at Blue Spring are consistent with a simple progression of water–rock reaction as reactive soil water infiltrates through the limestone and emerges in the ceiling of the cave as drip water.

5.2.2. Model assessment of prior calcite precipitation

None of these simulations described thus far implement any secondary calcite precipitation. Thus, the potential exists to explain the remaining range of the measured values (Fig. 2) by allowing this range of drip water to further evolve through carbonate precipitation. Several versions of this evolution are considered. First, if a completely pure $CaCO_3$ phase is allowed to form which excludes all Mg and Sr, the slope of the line formed by these nine simulated scenarios remains constant, as Ca is simply removed from the fluid (Fig. 9 – blue dotted line). This behavior is able to cap-

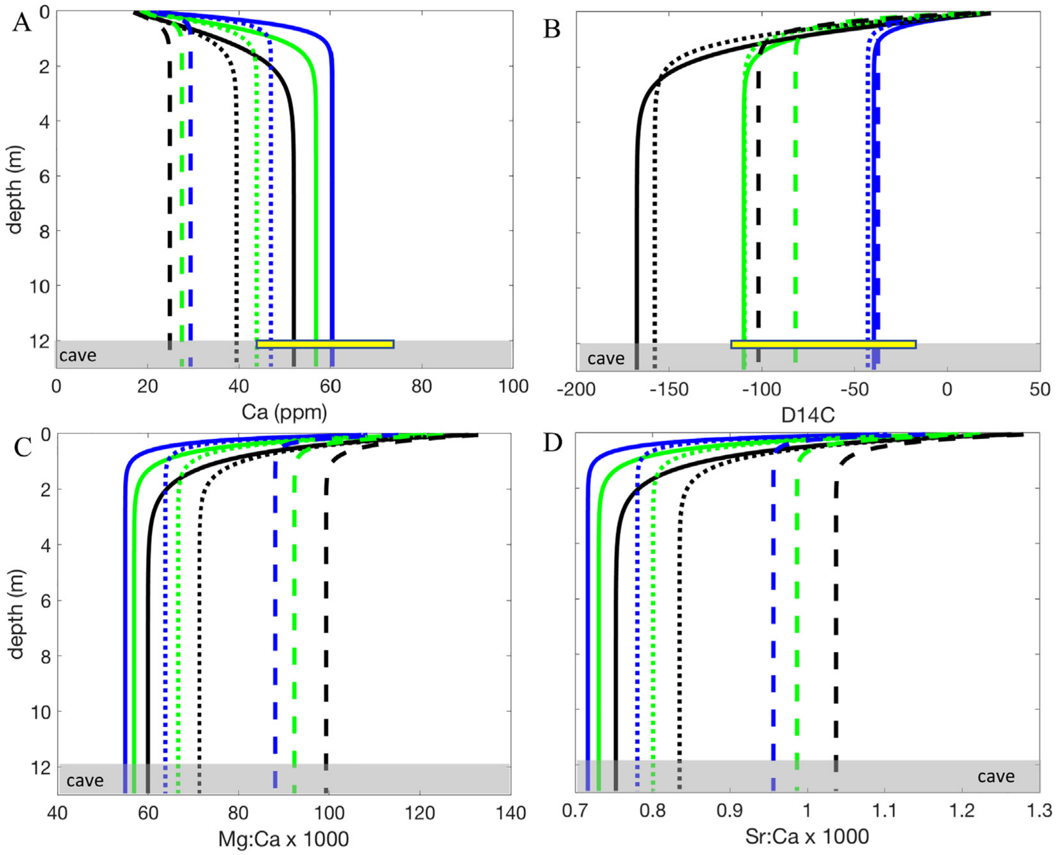

Fig. 8. CrunchTope simulations of (A) Ca^{2+} concentrations (ppm); (B) total inorganic fluid phase radiocarbon (‰); (C) dissolved Mg/Ca molar ratios (mmol/mol); (D) dissolved Sr/Ca molar ratios (mmol/mol). Pannels (A) and (B) are reproduced from Druhan et al., 2021). Colors indicate fast (black), moderate (green) and slow (blue) flow rates across a 13 m depth profile. Dilute, acidic fluid infiltrates across the top boundary at fixed flow rates with a chemical composition constrained by soil water monitoring data. The temperature is 13.5 °C and three influent pCO_2 values are implemented, high (solid line), mid (dotted line) and low (dashed line). The range of measured Ca^{2+} concentrations and radiocarbon DIC values in the measured drip waters are illustrated with yellow bars at 12 m depth (the ceiling of the cave).(For interpretation of the references to colour in this figure legend, the reader is referred to the web version of this article.)

ture an additional range of measured drip water ratios and offers a logical explanation for the variety of measurements which record the lowest Sr/Ca ratios in the natural system. Specifically, the mostly fracture-fed drips located in the Upper Pool Room (BSw5, BSw11, JENC1-4) align most closely in terms of their ln(Mg/Ca) and ln(Sr/Ca) with the dissolution-only water emerging from the limestone and precipitating varying amounts of pure carbonate (blue points and line, Fig. 9).

This relatively simple dissolution of the Blue Spring host limestone (Eq. (2)) with attendant precipitation of pure calcite creates a solution space, which is consistent with some of the Blue Spring drip waters. However, we note that a substantial number of drip water measurements record elevated Sr/Ca ratios relative to this trend line (Fig. 9). To begin to consider this variability, we also explore a range of secondary carbonates which form with the inclusion of Mg and Sr to varying extents (Table 2).

The choice of this range of values corresponds to the range of ratios measured in the 120,000–80,000 year-old stalagmite collected from the Cathedral Room, and so brackets a range of both low and high Mg and Sr incorporation directly observed in this cave system. The result is a range of model solutions that encapsulate some of the measured Mg/Ca and Sr/Ca ratios of the drip water, as this variety of secondary carbonate phases are allowed to form from the original fluid exiting the base of the limestone at the cave boundary. For illustration purposes, we utilize the lowest Mg/Ca and Sr/Ca values for this fluid emerging into the cave as a starting point (Fig. 9), though we note that lines of this slope could also extend from any value illustrated in the solution set corresponding to the nine simulations used to generate the range of values produced by limestone dissolution (Fig. 8). Precipitation of carbonate of compositions that are similar to what is measured in the speleothem elevates Sr/Ca and Mg/Ca of drip water to values that are in range of some of the measurement of diffuse drip sites BSw4 and BSw10 (red and green lines, Fig. 9). Essentially, the results of these calculations indicate that the drip water measurements falling between and around the dashed blue and solid green lines on Fig. 9 can be explained through a combination of limestone dissolution and then precipitation of either pure secondary carbonate or secondary carbonate with trace element phases

Please cite this article in press as: Oster J. L., et al. A reactive transport approach to modeling cave seepage water chemistry II: Elemental signatures. *Geochim. Cosmochim. Acta* (2021), https://doi.org/10.1016/j.gca.2021.06.040

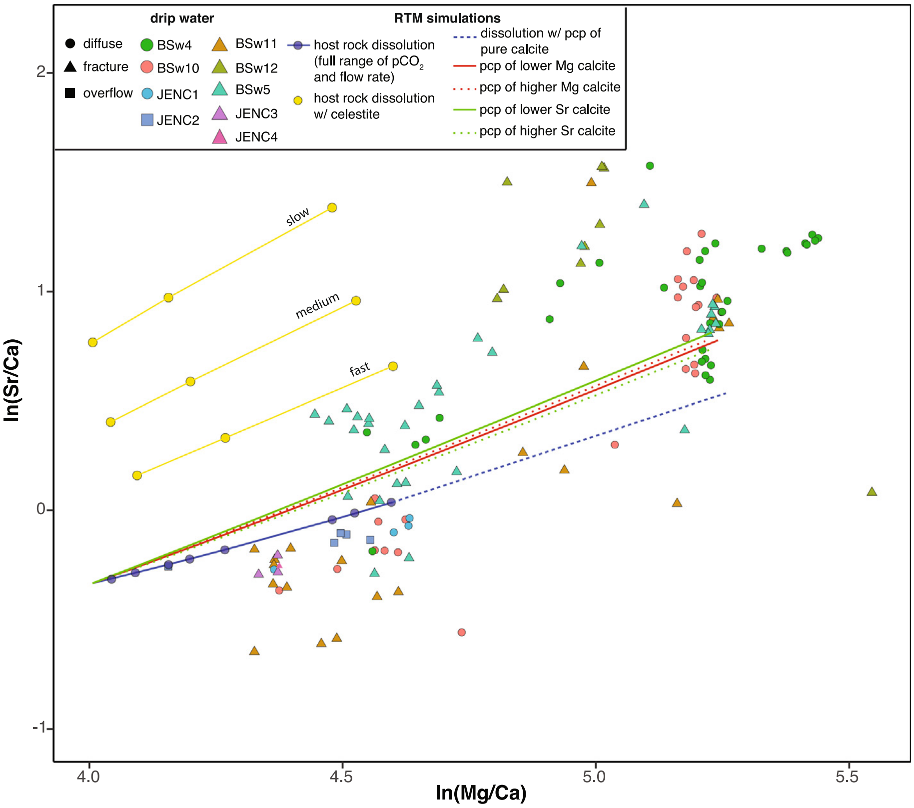

Fig. 9. Comparison of drip water data with RTM output in Ln(Mg/Ca) versus Ln(Sr/Ca) space. Drip water data are coded by drip site (color) and drip type (shape). Model output shows composition of water emerging into the cave following dissolution of limestone under varying flow rate and pCO2 (solid blue line) and undergoing pure calcite precipitation upon emergence into the cave boundary condition (dashed blue line). Red and green lines illustrate range of results if the secondary calcite phase precipitated within the cave boundary condition encompasses the range of Mg/Ca and Sr/Ca measured in the Blue Spring Cave stalagmite. Yellow dots/lines represent composition of water emerging into the cave having dissolved variable amounts of a "celestite" phase, following the same nine combinations of flow rate and pCO_2 as are implemented in the other model simulations. Model runs with the same flow rate are connected by yellow lines. Of these, the model runs with the highest ln(Mg/Ca) and ln(Sr/Ca) along each line, have the lowest starting soil pCO_2. (For interpretation of the references to colour in this figure legend, the reader is referred to the web version of this article.)

Table 2
Range of Mg/Ca and Sr/Ca ratios considered in the formation of secondary carbonates from the drip water solute compositions derived from the 1D reactive transport model.

Carbonate	(Mg/Ca)×1000 molar ratio	(Sr/Ca)×1000 molar ratio
CaCO3 + Mg + Sr	2.190	0.133
CaCO3 + lowMg + Sr	1.379	0.133
CaCO3 + highMg + Sr	2.99	0.133
CaCO3 + Mg + lowSr	2.190	0.010
CaCO3 + Mg + highSr	2.190	0.166

similar to what we have measured in the Blue Spring speleothem.

As calcite precipitation is implemented in the model, we prescribe the starting composition of the infiltrating fluid and the trace element to calcium ratios within the secondary carbonate (Table 2). We do not directly prescribe partition coefficients for each trace element in the model. The fluid phase trace element ratios evolve such that secondary calcite of this composition is formed. The partition coefficients are thus variables that emerge from the model rather than fixed parameters prescribed at the start of the simulation. We can compute these from the precipitating solid and the evolving fluid output from the model. When we do this, we calculate partition coefficients for Mg (D_{Mg}) that range from 0.01 to 0.04 for precipitation of calcite with moderate Mg and Sr (following the first line in Table 2), with slightly lower values for precipitation of calcite with lower Mg/Ca (0.01–0.03), and slightly higher

Please cite this article in press as: Oster J. L., et al. A reactive transport approach to modeling cave seepage water chemistry II: Elemental signatures. *Geochim. Cosmochim. Acta* (2021), https://doi.org/10.1016/j.gca.2021.06.040

values for precipitation of calcite with higher Mg/Ca (0.01–0.06). The values of D_{Sr} we calculated for precipitation of calcite with moderate Mg and Sr (Table 2) range from 0.06 to 0.19, with slightly lower values for precipitation of calcite with lower Sr/Ca (0.04–0.14), and slightly higher values for precipitation of calcite with higher Sr/Ca (0.08–0.23). These values decrease as the fluid evolves and precipitates calcite. Although our approach of holding the calcite trace element compositions constant is idealized relative to the cave setting, the ranges of values for D_{Mg} and D_{Sr} that we calculate are similar to those calculated from drip waters and calcite from modern cave environments covering a range of climates and host rock types (0.011 to 0.039 for D_{Mg}, and 0.037 to 0.34 for D_{Sr}) (Wassenburg et al., 2020).

In total, these simulations suggest that a reasonable representation of some of the measured Blue Spring drip water element ratios can be attributed to a combination of limestone dissolution and precipitation of a secondary carbonate phase that is either pure $CaCO_3$ or incorporates the range of Mg and Sr reflected in direct measurements of Blue Spring speleothems (Table 2). It is critical to recognize that this result does not invoke the need for PCP to occur prior to the emergence of the fluid into the cave as drip water but that these waters evolve through PCP after encountering the cave boundary condition. We maintain that based on the model results of the companion paper (Druhan et al., 2021), the balance between calcium concentrations and radiocarbon values cannot accommodate substantial PCP in the host rock (Fig. 8). Thus, the combination of these observations suggests that the Mg/Ca and Sr/Ca ratios measured in some Blue Spring drip water samples reflect varying extents of PCP that occur as the drip water is exposed to the cave air in the interval between emergence from the overlying host rock and sampling. However, this exercise also demonstrates that the range of Mg and Sr incorporation reasonably suggested to occur in secondary carbonates in the Blue Spring system does not allow for substantial further enrichment of Sr relative to Mg in the fluid. Instead, the range of mineral stoichiometries tested (Table 2) creates a relatively narrow band of possible Sr/Ca, Mr/Ca pairs and in particular does not reproduce the highly elevated Sr/Ca ratios observed in some Blue Spring drip waters.

5.2.3. Incorporation of celestite

The observation of elevated Sr/Ca ratios, as well as the site-to-site variability in drip Sr/Ca, then requires an additional factor to reconcile the model and measurements. The diagenetic celestite that has been noted within the Monteagle Limestone (Handford, 1976) may provide a source of Sr that is distributed heterogeneously in the Blue Spring system such that it influences some of the drip sites at times, but not others. As an extension of the model, we consider whether or not such an additional factor could reasonably explain the Blue Spring drip water data by adding a unique celestite phase to the limestone in our simulations. Since we did not directly observe this phase or record its effects on solution chemistry we are left to rely on preexisting parameter values for solubility. Using the EQ3/6 database (Woolery 1992) parameters, the equilibrium coefficients for this representative celestite are specified as $\log K_{eq} = -5.6753$ at 0 °C and -5.6771 at 25 °C with linear temperature extrapolations in between. Based on these values and a sparingly low concentration of sulfate added to the influent boundary condition at the base of the soil, the fluid draining through the system is undersaturated; thus, dissolution adds both Sr and SO_4 to the aqueous phase. A rate constant of $\log k = -8.6$ regulates the speed of this dissolution, and the nine original model scenarios featuring three flow rates and three soil pCO_2 boundary conditions are rerun. The results of this test (yellow lines, Fig. 9) illustrate a wide range of elevated Sr/Ca ratios in the composition of drip water entering the cave from the host rock that is spread out even before any PCP is considered. Notably, these simulations cluster into three unique slopes when observed in ln(Mg/Ca) versus ln(Sr/Ca) space, differentiated by the flow rate of fluid through the limestone. The fastest fluid flow rate falls closer to the original simulations which omitted celestite. The slowest flow rate creates the most elevated Sr/Ca trend, as would be expected given that slower flow allows time for more dissolution of celestite as well as limestone. Within a given flow rate, the three values of soil pCO_2 create varying degrees of reactivity (lower Sr/Ca and Mg/Ca corresponds to a higher soil pCO_2 and thus more dissolution of limestone (yellow points, Fig. 9).

The incorporation of this celestite phase is speculative given that we have no information beyond reports of celestite in the Monteagle Limestone to directly document the distribution or reactivity of such a phase in the vicinity of Blue Spring Cave. However, the model provides an interesting opportunity to test whether or not the inclusion of this phase is feasible and would produce reasonable behavior. We find, without any tuning from literature-reported reaction parameters, that a celestite mineral would dissolve in these fluids. The result for our range of flow rates and soil pCO_2 values further indicates that if an analogous Sr rich phase is contributing to the signatures of some drip water, the magnitude of these ratios is largely driven by fluid flow rate, rather than the reactivity of the CO_2-charged fluid infiltrating from the upper soil surface. Drip sites from farther back in the cave, BSw12, BSw4, and BSw10 as well as some measurements of BSw5, align more closely with modeled waters that have dissolved some amount of the celestite phase (Fig. 9).

5.2.4. Evaluation of modeled water Ba/Ca

Finally, as an additional independent check on the validity of these data-model comparisons, we incorporated a trace amount of Ba into the simulations. Barium was not directly measured in the supporting batch dissolution experiments and exists in very small quantities in the limestone, resulting in a measured limestone Ba/Ca ratio of 0.001 mmol/mol (Table 1). The average Ba/Ca ratio measured in the lysimeters above the cave system is much higher, with an average value of 0.44 mmol/mol. Using these two measurements, we incorporated Ba into the simulations with no further adjustment to any aspect of the model. The results (blue points, line on Fig. 10) generally support the fidelity of this model framework as a representation of the Blue Spring system. Notably, the range of Ba/Ca vs. Sr/Ca ratios obtained from the nine model scenarios

Please cite this article in press as: Oster J. L., et al. A reactive transport approach to modeling cave seepage water chemistry II: Elemental signatures. *Geochim. Cosmochim. Acta* (2021), https://doi.org/10.1016/j.gca.2021.06.040

without any further PCP indicate that (1) the modeled Sr/Ca values are far too low and (2) the Ba/Ca ratios are far too high relative to observations. To explore the latter possibility, we conducted a simulation using limestone with a Ba concentration of zero; this produces results which are indistinguishable from the original trend. Thus, it is not possible to decrease the simulated Ba/Ca ratio of fluids through some alteration of the limestone stoichiometry. However, it is possible that the Ba/Ca of the inflowing soil water in the model, which is based on the mean Ba/Ca in water measured in the deepest lysimeter, is higher than what is actually infiltrating into the limestone. The soils above Blue Spring Cave are rich in clay and thus have the potential to hold relatively high concentrations of cations. The average Ba/Ca in the soil water decreases with depth between the two deepest lysimeters (average of 1.03 mmol/mol in L04 at 50 cm depth versus 0.44 in L05 at 90 cm depth). Thus, it is possible that Ba/Ca continues to decrease deeper into the soil profile as water enters the epikarst. The influence of decreased initial fluid Ba/Ca on the model outcome is demonstrated by a dashed line on Fig. 10; this produces modeled Ba/Ca in the range of most of the measured drip water values.

To address the excess Sr in the measured drip water compared to the model, we return to the experimental incorporation of a celestite phase. The same parameterization used in Fig. 9 returns drip water ratios in ln(Sr/Ca) vs. ln(Ba/Ca) space that are in much closer agreement with the measured values with respect to Sr/Ca (yellow points and lines, Fig. 10), which further improves when we reduce the Ba/Ca of infiltrating soil water, as above (dashed black lines, Fig. 10). Thus, overall we can suggest three lines of evidence that support the inference that Sr/Ca is influenced to varying degrees by a heterogeneously distributed Sr-rich phase: (1) Sr/Ca in the batch dissolution experiments showed excellent agreement between measured and modeled values indicating that the sample of limestone used did not produce additional Sr solubilization; (2) Sr/Ca values in some (but not all) drip waters are highly elevated relative to both Mg/Ca and Ba/Ca ratios; (3) the fluid draining through the Blue Spring host rock is undersaturated with respect to celestite.

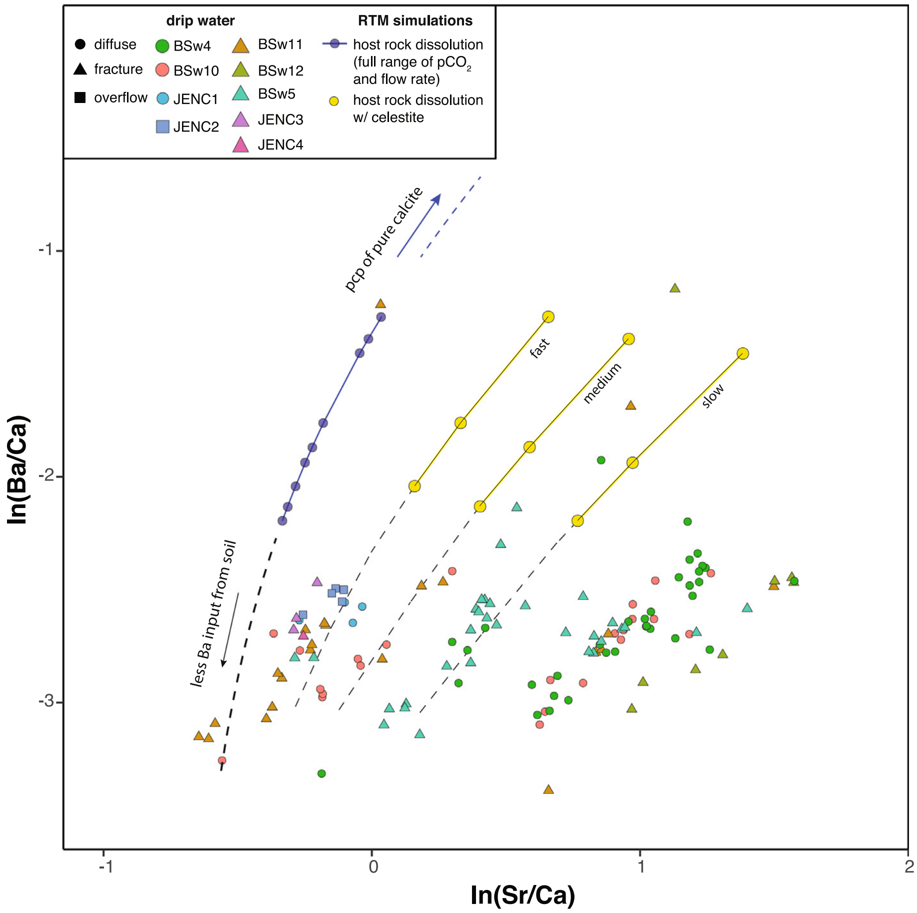

Fig. 10. Comparison of drip water data with RTM output in Ln(Sr/Ca) versus Ln(Ba/Ca) space. Drip water data are coded by drip site (color) and drip type (shape). Model output shows composition of water emerging into the cave following dissolution of limestone under varying flow rate and pCO$_2$ (solid blue line). Dashed lines illustrate modeled water composition after undergoing precipitation of pure calcite (blue, higher values) and assuming a lower initial Ba/Ca from the soil boundary condition (black, lower values). As with Fig. 9, yellow dots/lines represent composition of water emerging into the cave having dissolved variable amounts of a "celestite" phase. Dashed lines extend these trajectories to lower initial Ba/Ca values from the soil boundary condition. (For interpretation of the references to colour in this figure legend, the reader is referred to the web version of this article.)

It is further apparent that different drip sites fall on different lines defined by the overall amount of Sr (Figs. 4 and 10), making it possible to distinguish drip sites with different amounts of Sr input from a potential celestite phase. Similar to observations from the comparison of Sr/Ca with Mg/Ca, drip sites from the Upper Pool Room (BSw11 and JENC drips) most closely align with modeled ratios for waters exiting the limestone, then undergoing variable amounts of PCP, with minimal dissolution of celestite. This is consistent with more rapid flow through the limestone. Site BSw11 occasionally displays higher Sr/Ca; site BSw5, which is located on the opposite site of the Upper Pool Room displays slightly higher to much higher Sr/Ca. These observations indicate that flow paths leading to the Upper Pool Room experience fast to medium flow rates and/or encounter relatively low amounts of celestite. Sites BSw4 and BSw10, which are located between the Upper Pool Room and the Cathedral Room display generally higher Sr/Ca, indicating slower flow through the limestone and more contact with celestite along the flow path. These sites exhibit less variable drip rates than the Upper Pool Room drips and are active throughout the year. Thus, a slower flow rate, as suggested by the model, is consistent with observations shown here as well as with the relatively low variability observed in the $\delta^{13}C$ of DIC indicated across these drip sites (Druhan et al., 2021). Site BSw12 located farthest from the cave entrance at the back of the Cathedral Room has the highest Sr/Ca. The $\delta^{13}C$ values noted in BSw12 drip water DIC (Druhan et al., 2021), are highly variable and consistent with more rapid, fracture-fed flow through the host rock, similar to sites BSw11 and BSw5. This suggests that the high Sr/Ca at this site is more attributable to spatial heterogeneities within the host rock that result in more water contact with celestite (or a comparably reactive high Sr phase) along the flow path. In many ways, this approach is analogous to that of Tremaine and Froelich, 2013 and Wassenburg et al., (2020) who modeled PCP relationships between drip water Mg/Ca and Sr/Ca by setting a portion of the limestone to dolomite in the dissolved host rock (e.g. Fig. 5). Our approach differs in that we are dissolving a Sr-rich phase that does not influence carbonate saturation within the drip water.

5.3. Disentangling evidence of mineral dissolution and PCP in cave drip waters

Comparing the RTM results and drip water measurements from the Blue Spring system indicates that element to calcium ratios are controlled by a combination of multiple mineral dissolution reactions within the host rock as well as PCP. Our modeling of both carbon isotopes (Druhan et al., 2021) and element to calcium ratios at Blue Spring strongly suggests that the occurrence of PCP is related to in-cave processes rather than processes within the host rock and that the extent of PCP in the cave is not significant enough to strongly impact the calcium concentrations within the drip waters. Rather, it only influences the ratios of Mg, Sr, and Ba with calcium. This finding is similar to observations based on carbon isotopes of cave drip waters in Texas (Meyer et al., 2014), and comparisons of coeval speleothem $\delta^{13}C$ from a global database that relates $\delta^{13}C$ to drip interval at the stalagmite growth site (Fohlmeister et al., 2020). However, the model also indicates that the range of measured drip water Mg/Ca and Sr/Ca cannot be explained by similarly simple variations in the amount of limestone dissolved, the amount of PCP occurring, or the composition of the secondary calcite that is being precipitated, given the measured range of Mg and Sr concentrations within both the limestone and the secondary carbonate at Blue Spring. Rather, our measurements indicate that non-limestone phases, such as celestite related to diagenesis of the host limestone, exert an influence on drip water chemistry and that these phases are likely heterogeneously distributed through the host rock. Our modeling supports these observations and suggests that interactions of seepage waters with these diagenetic phases are necessary to explain the range of Mg/Ca and Sr/Ca observed in the Blue Spring drip water. In contrast, modeled Ba/Ca is a much simpler mixture between a high Ba fluid infiltrating through a uniformly Ba-depleted limestone, with no apparent input from additional phases. The modeled drip water Ba/Ca values are generally higher than the measured drip water Ba/Ca. As described above, this discrepancy cannot be resolved through lowering the Ba concentration of the host limestone. However, if we lower the initial Ba/Ca of the fluid flowing in from the soil at the upper boundary condition, we obtain modeled drip water Ba/Ca that is similar to what is measured (Fig. 10). Thus, we hypothesize that the measured Ba/Ca in deep lysimeter water may be too high relative to what is actually infiltrating into the cave via the seepage water.

In order for speleothem Mg/Ca and Sr/Ca to offer a straightforward tracking of PCP changes and thus provide a record of past rainfall variability, Mg and Sr must be supplied by a single or dominant source, namely the host limestone unit (Sinclair et al., 2012; Tremaine and Froelich, 2013). In many cave systems, including Blue Springs Cave, the single-source rule does not apply for Mg, which can also be variably supplied by dolomite phases within the host rock (e.g. Tremaine and Froelich, 2013; Oster et al., 2014, 2017; Oster et al., 2020), or sea salt aerosols (e.g. Baldini et al., 2015; Tremaine et al., 2016; Noronha et al., 2017). Likewise, Sr incave waters can be derived from sources besides the host limestone, including sea spray, dust, and non-carbonate components of the soil or host rock. Contributions from these phases can often be tracked through measurement of Sr-isotope ratios ($^{87}Sr/^{86}Sr$) (Banner et al., 1996; Goede et al., 1998; Ayalon et al., 1999; Bar-Matthews et al., 1999; Oster et al., 2009; 2014). With regard to the hypothesized inclusion of celestite in the Blue Spring system, we have a source rich in Sr that is readily dissolvable and influences different flow paths to different degrees. The existence of heterogeneously distributed dolomite and celestite within the Blue Spring system leads to a complex relationship between infiltration (or net rainfall) and drip water Mg/Ca and Sr/Ca, as our model suggests that the degree of celestite dissolution can respond to flow rate (Figs. 9 and 10). It is possible that the large changes in net rainfall that are especially apparent between March 2014 and September 2015 caused variations in the dissolution of these diagenetic phases and/or physical changes in flow paths that caused large variations in drip water Mg/Ca and Sr/Ca. If this is the case, the drip sites were influenced in different ways and to varying degrees. However, adjacent sites, such as BSw4 and BSw10 which are both characterized as diffuse flow sites and generally indicate high Mg/Ca and Sr/Ca consistent with enhanced dissolution of dolomite and celestite, behaved similarly (Figs. 3–5). This suggests, at least on the scale of a few meters, that drip sites are likely sampling similar flow paths and should respond to changes in effective rainfall in similar ways. Thus, our results highlight the necessity to understand drip water chemistry close to the location of speleothem collection when conducting monitoring in support of paleoclimate interpretations, given the spatial complexities that can arise in karst systems. Furthermore, adequate understanding of the variations in drip chemistry may require application of geochemical models that allow for the consideration of heterogeneously distributed accessory mineral phases.

Our model-data observation further indicates, in the Blue Spring system, rather than Mg/Ca and Sr/Ca, Ba/Ca may provide the most straightforward metric for tracking changes in PCP and therefore net rainfall. Ba/Ca is sometimes included as part of multi-proxy speleothem studies, closely tracks Sr/Ca in speleothems and drip water and is often discussed as a PCP-sensitive proxy (Oster et al., 2009; Warken et al., 2019). In the Blue Spring system Ba/Ca does not appear to be influenced by a heterogeneously distributed secondary source, as all drip sites generally respond coevally to environmental changes and display very similar values (Fig. 3). Measured drip water values plot on a slope that is similar to the inferred PCP slope (Sinclair et al., 2012) in a diagram of ln(Sr/Ca) versus ln(Ba/Ca) (Fig. 2), suggesting that Ba/Ca is primarily influenced by PCP. Variations in ln(Ba/Ca) appear to track net rainfall (Fig. 3). Across all measurements, Pearson's correlation coefficients between ln(Ba/Ca) and monthly net rainfall are negative and weakly significant ($r = -0.24$, $p = 0.01$, $n = 107$), compared with insignificant correlations of net rainfall with ln(Sr/Ca) or ln(Mg/Ca). When we compute monthly averages of ln(Ba/Ca) and net rainfall across the entire dataset, the correlations substantially improve ($r = -0.57$, $p = 0.05$, $n = 12$) (Fig. 11). Similar monthly averages of ln(Sr/Ca) and ln(Mg/Ca) do not show significant correlations with net rainfall. Further, there is no clear indication of a relationship between drip water Ba/Ca and the seasonal pattern of cave ventilation, in which we would expect more PCP to occur in the winter. This suggests that PCP in Blue Spring appears to respond to rainfall and that changes in PCP in response to varying net rainfall occur consistently throughout the cave. That this relationship is most clearly seen in the record of drip water Ba/Ca indicates that measured Ba/Ca in stalagmites will be the most accurate proxy for reconstructing PCP, and therefore past rainfall amounts, at Blue Spring Cave. We therefore highlight the need for further investigation into the cycling of Ba in soil-cave systems to evaluate speleothem Ba/Ca as a paleoclimate proxy across climate gradients.

6. CONCLUSIONS

We have utilized the reactive transport model CrunchTope to explore the primary drivers behind spatiotemporal variations in drip water chemistry at Blue Spring Cave in Tennessee. Building on our exploration of stable and radioactive carbon isotopes in Blue Spring (Druhan et al., 2021), we have used coordinated measurements of elemental compositions of soil waters and host rocks to evaluate the influence of mineral dissolution and precipitation on drip water chemistry. Consistent with observations from the modeling of carbon isotopes, we find that the range of element to calcium ratios (Mg/Ca, Sr/Ca, Ba/Ca) measured in Blue Spring drip water can be mostly explained through dissolution of limestone along the flow path with variable amounts of PCP occurring after drip water emerges into the cave. The tracking of the element to calcium ratios highlights an additional spatial variability in drip water chemistry within this cave that is not apparent from observations of carbon isotopes. Specifically, comparison of observations with model outputs suggests that drip waters are interacting with a soluble celestite phase within the host rock, and that there is a large degree of heterogeneity among flow paths in the amount of interaction with this phase. Spatial variations in the Sr/Ca as well as the Mg/Ca among drip waters is consistent with previous observations of diagenetic celestite and dolomite within the Monteagle Limestone, which hosts Blue Spring. However, the presence of reactive high-Mg calcite from crinoids within the limestone is shown to not have a significant influence on drip water Mg/Ca. The occurrence and non-uniform distribution of the diagenetic phases also undermines the use of Sr/Ca and Mg/Ca in Blue Spring stalagmites as clear proxies for PCP. In contrast, we find that Ba/Ca varies consistently and contemporaneously across the cave, and responds to changes in net rainfall. Thus, we recommend Ba/Ca as the most straightforward proxy for PCP and effective rainfall amount, in this cave system.

Our coupled model-data analysis at Blue Spring underscores the need to fully explore each cave system through modern observations before or in parallel with the interpretation of speleothem proxy records as this work can identify the proxies that most closely reflect environmental parameters such as infiltration/rainfall amount. Furthermore, this work uncovers clear spatial variability in cave drip water chemistry that can overprint drip character (i.e. whether a drip is fed by fracture versus diffuse flow from the host rock) that occurs due to heterogeneity of mineral phases in the host rock. This highlights the need to understand the controls on drip water chemistry at or near the site of speleothem collection. Reactive transport models that have been parameterized for modern cave systems provide a powerful tool for evaluating speleothem data, exploring which combinations of external environment and cave conditions can best explain observations from all proxies and producing more robust paleoclimate reconstructions.

Please cite this article in press as: Oster J. L., et al. A reactive transport approach to modeling cave seepage water chemistry II: Elemental signatures. *Geochim. Cosmochim. Acta* (2021), https://doi.org/10.1016/j.gca.2021.06.040

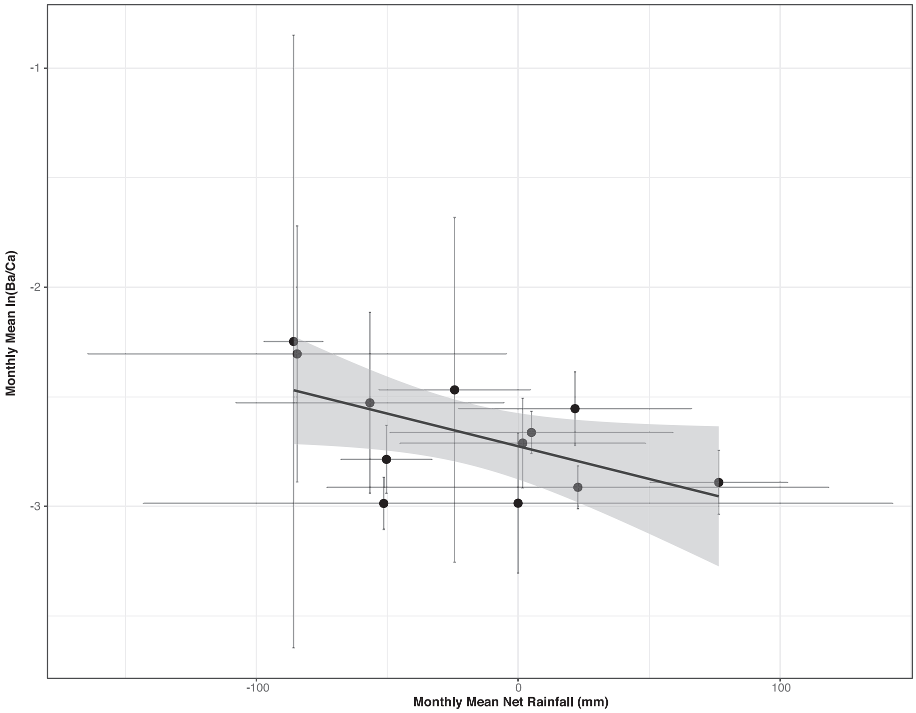

Fig. 11. Monthly mean net rainfall against monthly mean Ln(Ba/Ca) across all drip sites with standard deviations with linear regression (black line) and 95% confidence interval (gray shading).

7. DATA AVAILABILITY

Cave monitoring data are available as supplemental tables to this and the companion paper (Druhan et al., this volume. Data are archived through the USGS ScienceBase (https://doi:10.5066/P90OTSDY) and also in the Cave Monitoring Database (https://cave-monitoring.org). CrunchTope input files are available as supplementary information and the software is open source.

Declaration of Competing Interest

The authors declare that they have no known competing financial interests or personal relationships that could have appeared to influence the work reported in this paper.

ACKNOWLEDGEMENTS

This work was supported by grants from the National Science Foundation (EAR-1600766 to JLO and EAR-1600931 to JLD) and the Cave Research Foundation. We thank Lonnie Carr for access to Blue Spring Cave and support of the research and Hal Love for guidance in the original field work. We also acknowledge countless field assistants from Vanderbilt University as well as Jaressa Hawkins, Ella Halbert, Nancy Hoang, and Cecily Shi (JENC), and Angela Eeds of the School for Science and Math at Vanderbilt. We thank two anonymous reviewers, Darrel Tremaine and Jens Fohlmeister for valuable comments on this manuscript as well as Associate Editor Frank McDermott for handling the manuscript. Any use of trade, firm, or product names is for descriptive purposes only and does not imply endorsement by the U.S. Government.

APPENDIX A. SUPPLEMENTARY MATERIAL

Supplementary data to this article can be found online at https://doi.org/10.1016/j.gca.2021.06.040.

REFERENCES

Ayalon A., Bar-Matthews M. and Kaufman A. (1999) Petrography, strontium, barium and uranium concentrations, and strontium and uranium isotope ratios in speleothems as paleoclimate proxies: Soreq Cave, Israel. *The Holocene* **9**, 715–722.

Baker A., Bradley C., Phipps S. J., Fischer M., Fairchild I. J., Fuller L., Spötl C. and Azcurra C. (2012) Millennial-length forward models pseudoproxies of stalagmite δ^{18}O: an example from NW Scotland. *Clim. Past* **8**, 1153–1167.

Baldini L. M., McDermott F., Baldini J. U. L., Arias P., Cueto M., Fairchild I. J., Hoffmann D. L., Mattey D. P., Muller W., Nita D., Ontanon R., Garcia-Monco C. and Richards D. A. (2015) Regional temperature, atmospheric circulation, and sea-ice variability within the Younger Dryas Event constrained using a stalagmite from northern Iberia. *Earth Planet. Sci. Lett.* **419**, 101–110.

Banner J. L., Musgrove M., Asmerom Y., Edwards R. L. and Hoff J. A. (1996) High-resolution temporal record of Holocene ground-water chemistry: tracing links between climate and hydrology. *Geology* **24**, 1049–1053.

Banner J. L., Guilfoyle A., James E. W., Stern L. A. and Musgrove M. (2007) Seasonal variations in modern speleothem calcite growth in Central Texas, U.S.A. *J. Sedimentary Res.* **77**, 615–622.

Bar-Matthews M., Ayalon A., Kaufman A. and Wasserburg G. J. (1999) The Eastern Mediterranean paleoclimate as a reflection of regional events: Soreq cave, Israel. *Earth Planet. Sci. Lett.* **166**, 85–95.

Please cite this article in press as: Oster J. L., et al. A reactive transport approach to modeling cave seepage water chemistry II: Elemental signatures. *Geochim. Cosmochim. Acta* (2021), https://doi.org/10.1016/j.gca.2021.06.040

Busenberg E. and Plummer L. N. (1989) Thermodynamics of magnesian calcite solid-solutions at 25°C and 1 atm total pressure. *Geochim. Cosmochim. Acta* **53**, 1189–1208.

Chou K., Garrels R. M. and Wollast R. (1989) Comparative study of the kinetics and mechanisms of dissolution of carbonate minerals. *Chem. Geol.* **78**, 269–282.

Cross M., McGee D., Broecker W. S., Quade J., Shakun J. D., Cheng H., Lu Y. and Edwards R. L. (2015) Great Basin hydrology, paleoclimate, and connections with the North Atlantic: a speleothem stable isotope and trace element record from Lehman Caves, NV. *Quat. Sci. Rev.* **127**, 186–198.

Driese S. G., Srinivasan K., Mora C. I. and Stapor F. W. (1994) Paleoweathering of Mississippian Monteagle Limestone preceding development of a lower Chesterian transgressive systens tract and sequence boundary, middle Tennessee and northern Alabama. *Geol. Soc. Am. Bull.* **106**, 866–878.

Druhan J., Lawrence C., Covey A. K., Giannetta M. G. and Oster J. L. (2021) A reactive transport approach to modeling cave seepage water chemistry I: Carbon isotope transformations. *Geochim. Cosmochim. Acta*. doi.10.1016/j.gca.2021.06.041.

Druhan J. L., Guillon S., Lincker M. and Arora B. (2020) Stable and radioactive carbon isotope partitioning in soils and saturated systems: a reactive transport modeling benchmark study. *Comput. Geosci.*, 1–11.

Fairchild I. J., Borsato A., Tooth A. F., Frisia S., Hawkesworth C., Huang Y., McDermott F. and Spiro B. (2000) Controls on trace element (Sr-Mg) compositions of carbonate cave waters: implications for speleothem climatic records. *Chem. Geol.* **166**, 255–269.

Fairchild I. J. and Treble P. C. (2009) Trace elements in speleothems as recorders of environmental change. *Quat. Sci. Rev.* **28**, 449–468.

Fohlmeister J., Voarinstsoa N. R. G., Lechleitner F. A., Boyd M., Brandstätter M. J., Jacobson M. J. and Oster J. L. (2020) Main controls on the stable carbon isotope composition of speleothems. *Geochim. Cosmochim. Acta* **279**, 67–87.

Goede A., McCulloch M., McDermott F. and Hawkesworth C. (1998) Aeolian contribution to strontium and strontium isotope variations in a Tasmanian speleothem. *Chem. Geol.* **149**, 37–50.

Handford C. R. (1976) Sedimentology and diagenesis of the Monteagle Limestone (Upper Mississippian) – a high energy oolitic carbonate sequence in the southern Appalachian Mountains PhD Dissertation. Louisiana State University.

Huang Y. and Fairchild I. J. (2001) Partitioning of Sr^{2+} and Mg^{2+} into calcite under karst analogue experimental conditions. *Geochim. Cosmochim. Acta* **65**, 47–62.

Johnson K. R., Hu C., Belshaw N. S. and Henderson G. M. (2006) Seasonal trace element and stable isotope variations in a Chinese speleothem: the potential for high-resolution paleomonsoon reconstruction. *Earth Planet. Sci. Lett.* **244**, 394–407.

Liu Y.-H., Henderson G. M., Hu C.-Y., Mason A. J., Charnley N., Johnson K. R. and Xiem S.-C. (2013) Links between the East Asian monsoon and North Atlantic climate during the 8,200 year event. *Nature Geosci.* **6**, 117–120.

Lumsden D. N., Norman C. D. and Reid B. J. (1983) The Monteagle Limestone (Mississippian) in north central Tennessee: petrology, porosity, and subsurface geology. *Southeastern Geol.* **24**, 39–50.

Matthews L. E. and Walter B. (2010). *Blue Spring Cave*. National Speleological Society.

Meyer K. W., Feng W., Breecker D. O., Banner J. L. and Guilfloyle A. (2014) Interpretation of speleothem calcite $\delta^{13}C$ variations: evidence from monitoring soil CO_2, drip water, and modern speleothem calcite in central Texas. *Geochim. Cosmochim. Acta* **142**, 281–298.

Miorandi R., Borsato A., Frisia S., Fairchild I. J. and Richter D. K. (2010) Epikarst hydrology and implications for stalagmite capture of climate changes at Grotta di Ernesto (NE Italy): results from long-term monitoring. *Hydrol. Process.* **24**(21), 3101–3114.

Noronha Alexandra L., Hardt Benjamin F., Banner Jay L., Jenson John W., Partin Judson W., James Eric W., Lander Mark A. and Bautista Kaylyn K. (2017) Trade winds drive pronounced seasonality in carbonate chemistry in a tropical Western Pacific island cave—implications for speleothem paleoclimatology. *Geochem., Geophys., Geosyst.* **18**(1), 384–399.

Oster J. L., Montañez I. P. and Kelley N. P. (2012) Response of a modern cave system to large seasonal precipitation variability. *Geochim. Cosmochim. Acta* **91**, 92–108.

Oster J. L., Montañez I. P., Mertz-Kraus R., Sharp W. D., Stock G. M., Spero H. J., Tinsley J. and Zachos J. C. (2014) Millennial-scale variations in western Sierra Nevada precipitation during the last glacial cycle MIS 4/3 transition. *Quat. Res.* **82**, 236–248.

Oster J. L. J., Sharp W. D., Covey A. K., Gibson J., Rogers B. and Mix H. (2017) Climate response to the 8.2 kyr event in Coastal California. *Sci. Rep.* **7**, 3886.

Oster J. L., Montañez I. P., Sharp W. D. and Cooper K. M. (2009) Late Pleistocene droughts during deglaciation and Arctic warming. *Earth Planet. Sci. Lett.* **288**, 434–443.

Oster J. L., Weisman I. E. and Sharp W. D. (2020) Multi-proxy stalagmite records from northern California reveal dynamic patterns of regional hydroclimate over the last glacial cycle.. *Quaternary Science Reviews* **241**, 106411.

Owen R., Day C. C. and Henderson G. M. (2018) CaveCalc: a new model for speleothem geochemistry and isotopes. *Comput. Geosci.* **119**, 115–122.

Parkhurst D. L. and Appelo C. A. J. (1999) User's guide to PHREEQC (Version 2): A computer program for speciation, batch-reaction, one-dimensional transport, and inverse geochemical calculations. Water Resources Investigations Report 99-4259.

Paton C., Hellstrom J., Woodhead J. and Hergt J. (2011) Iolite: Freeware for the visualization and processing of mass spectrometric data. *J. Anal. Atomic Spectrom.* **26**, 2508–2518.

Richards J. (2018) Map of Blue Spring Cave, White County, Tennessee. https://www.rchrds.org/tennesseecarto/2018/1/9/blue-spring-cave.

Ronay E. R., Breitenbach S. F. M. and Oster J. L. (2019) Sensitivity of speleothem records in the Indian Summer Monsoon region to dry season infiltration. *Sci. Rep.* **9**, 5091.

Rutlidge H., Baker A., Marjo C. E., Andersen M. S., Graham P. W., Cuthbert M. O., Rau G. C., Roshan H., Markowska M., Mariethoz G. and Jex C. (2014) Dripwater organic matter and trace element geochemistry in a semi-arid karst environment: Implications for speleothem paleoclimatology. *Geochim. Cosmochim. Acta* **135**, 217–230.

Sinclair D., Banner J. L., Taylor F. W., Partin J., Jenson J., Mylroie J., Goddard E., Quinn T., Jocson J. and Miklavic B. (2012) Magnesium and strontium systematics in tropical speleothems from the Western Pacific. *Chem. Geol.* **294–295**, 1–17.

Steefel C. I., Appelo C. A. J., Arora B., Jacques D., Kalbacher T., Kolditz O. and Molins S. (2015) Reactive transport codes for subsurface environmental simulation. *Comput. Geosci.* **19**(3), 445–478.

Please cite this article in press as: Oster J. L., et al. A reactive transport approach to modeling cave seepage water chemistry II: Elemental signatures. *Geochim. Cosmochim. Acta* (2021), https://doi.org/10.1016/j.gca.2021.06.040

Steponaitis E. et al. (2015) Mid-Holocene drying of the U.S. Great Basin recorded in Nevada speleothems. *Quat. Sci. Rev.* **127**, 174–185.

Stoll H. M., Müller W. and Prieto M. (2012) I-STAL, a model for interpretation of Mg/Ca, Sr/Ca, and Ba/Ca variations in speleothems and its forward and inverse application on seasonal to millennial scales. *Geochem., Geophys., Geosyst.* **13**, Q09004.

Swingle G. D., Miller R. A., Luther E. T., Hardeman W. D., Fullerton D. S., Sykes C. R. and Garman R. K. (1966) Geologic map of Tennessee [East Central Sheet]. Tennessee Division of Geology, State Geologic Map SEC.

Tesoriero A. J. and Pankow J. F. (1996) Solid solution partitioning of Sr2+, Ba2+, and Cd2+ to calcite. *Geochim. Cosmochim. Acta* **60**, 1053–1063.

Tremaine D. M. and Froelich P. N. (2013) Speleothem trace element signatures: a hydrologic geochemical study of modern cave dripwaters and farmed calcite. *Geochim. Cosmochim. Acta* **121**, 522–545.

Tremaine Darrel M., Sinclair Daniel J., Stoll Heather M., Lagerström Mari, Carvajal Carlos P. and Sherrell Robert M. (2016) A two-year automated dripwater chemistry study in a remote cave in the tropical south Pacific: Using [Cl−] as a conservative tracer for seasalt contribution of major cations. *Geochim. Cosmochim. Acta* **184**, 289–310.

Warken S. F., Scholz D., Spötl C., Jochum K. P., Pajón J. M., Bahr A. and Mangini A. (2019) Caribbean hydroclimate and vegetation history across the last glacial. *Quat. Sci. Rev.* **218**, 75–90.

Wassenburg J. A., Riechelmann S., Schröder-Ritzrau A., Riechelmann D. F. C., Richter D. K., Immenhauser A., Terente M., Constantin S., Hachenberg A., Hansen M. and Scholz D. (2020) Calcite Mg and Sr partition coefficients in cave environments: Implications for interpreting prior calcite precipitation. *Geochim. Cosmochim. Acta* **269**, 581–596.

Willmot C., Rowe C. and Mintz Y. (1985) Climatology of the terrestrial seasonal water cycle. *J. Climatol.* **5**, 589–606.

Wong C. I., Banner J. L. and Musgrove M. (2011) Seasonal dripwater Mg/Ca and Sr/Ca variations driven by cave ventilation: Implications for and modeling of speleothem paleoclimate records. *Geochim. Cosmochim. Acta* **75**, 3514–3529.

Woolery T. (1992) A software package for geochemical modelling of aqueous systems: package overview and installation guide (version 7.0). Technical report, Lawrence Livermore National Laboratory. UCRL- MA-110662 PT.

Associate editor: F McDermott

Please cite this article in press as: Oster J. L., et al. A reactive transport approach to modeling cave seepage water chemistry II: Elemental signatures. *Geochim. Cosmochim. Acta* (2021), https://doi.org/10.1016/j.gca.2021.06.040